Two-dimensional electron–electron double resonance and electron spin–echo study of solute dynamics in smectics[a]

Jeff Gorcester, Shankar B. Rananavare, and Jack H. Freed
Baker Laboratory of Chemistry, Cornell University, Ithaca, New York, 14853-1301

Electron spin–echo (ESE) and two-dimensional electron–electron double resonance (2D ELDOR) experiments have been performed as a function of director orientation and temperature in the smectic A phase of the liquid crystal S2 for the spin–probe PD-tempone(2×10^{-3} M). Over the entire temperature range studied (288–323 K) we observe significant 2D ELDOR cross peaks only for $\Delta M_I = \pm 1$ indicative of ^{14}N spin–relaxation and negligible Heisenberg exchange. From the angular dependent ^{14}N spin–relaxation rates we obtain the dipolar spectral densities at the hyperfine (hf) frequency, whereas from a combination of ESE and 2D ELDOR we obtain the dipolar and Zeeman-dipolar spectral densities at zero frequency. The angular dependent spectral densities were successfully decomposed into their basic components in accordance with theory. The angular dependent spectral densities at the hf frequency are not predicted by a model of anisotropic rotational diffusion in a nematic orienting potential, but are consistent with predictions of a model due to Moro and Nordio of solute rototranslational diffusion in a McMillan-type potential. The angular dependence also indicates that order director fluctuations in the smectic phase are suppressed at frequencies on the order of 10 MHz. An additional contribution to solute reorientation due to cooperative hydrocarbon chain fluctuations is suggested to account for the behavior of the observed spectral densities at zero frequency. An evaluation of the relevance of several other dynamical models to this experimental work is also presented.

I. INTRODUCTION

A. Motional dynamics in liquid crystals

NMR and ESR have been extensively utilized to study solute dynamics in liquid crystalline media. The solute spin–probe experiences a potential associated with the anisotropic solvent–solute interaction. Rotational motion of the spin–probe is strongly influenced by this potential, and this in turn significantly influences spin–relaxation. In the simplest model the probe experiences a static orienting potential due to the equilibrium potential of mean torque[1,2] in the liquid crystal. Spin–relaxation induced by the resulting restricted rotational diffusion of the probe molecule in the presence of this orienting potential may be used to probe the dynamic structure in the anisotropic medium. A somewhat more sophisticated model would include anisotropy in the viscosity of the solvent.[1,2] More detailed models of solute dynamics also consider the translational diffusion of the spin–probe in the medium.[3–7] In particular, if there is positional ordering of the liquid crystalline molecules, as in smectic phases, there will be a coupling between translation and rotation as the probe experiences different regions of the smectic layers[7] or regions with different instantaneous properties (e.g., fluctuations[5]). In other words, the probe experiences a continuously variable local orienting potential, as it translates through the medium.

In liquid crystalline phases one must consider cooperative phenomena, which can influence the rotational dynamics of the spin–probe. The mechanism which has received the most attention is the hydrodynamic model of order director fluctuations (ODF) suggested by Pincus.[8] ODF arise from collective motions of the liquid crystalline molecules causing the director to fluctuate about its mean position. Many observations of nematic ODF have been reported[9–16] based on the $\omega^{1/2}$ Larmor frequency dependence of the NMR T_1 that was predicted by Pincus and others.[3,8,10,17,18] In the case of ESR, Polnaszek and Freed[1] estimated some time ago that the contributions of ODF to the CW linewidth would be negligible for spin–probes in nematics. NMR measurements in smectic mesophases have been fewer in number and the conclusions have been rather conflicting.[12,16,19,20] The theoretical results of Blinc et al.,[19] Marqusee et al.,[21] and Vold et al.[17] predict a linear dependence of nuclear T_1 on ω as a result of restricting ODF to the plane of the layered structure, i.e., to two dimensions. The field cycling NMR experiments of Mugele et al. on the smectic A phase of TBBA [terephthal-bis(butyl-aniline)] appear to support this prediction,[12] although it is not clear that these expressions should apply to a multilayered structure such as TBBA. The linear dependence in ω of smectic ODF is not so obvious from the more extensive theoretical work of Vilfan et al., but a marked deviation from nematic-like behavior is predicted at low frequencies.[18] Also important is the conclusion of Noack et al. that smectic ODF are significant only at frequencies between about 1 and 100 kHz.[16] Extensions of the arguments of Polnaszek and Freed[1] indicate that smectic ODF should not be important for ESR.

Another important mechanism is that of order parameter fluctuations (OPF) discussed by Freed[3] to explain some anomalies in ESR linewidth measurements[22] near the nematic–isotropic (NI) phase transition. The OPF model involves critical types of fluctuations in the orienting potential. OPF should not be significant away from the NI phase transitions. Anomalies observed in the ESR linewidths near the nematic–smectic A (NA) phase transition[5,6,23,24] have been

interpreted in terms of a somewhat related model involving critical fluctuations of the smectic director which modifies the orientational relaxation of the spin–probe.[5,23,25] It has, however, been proposed that away from such phase transitions a somewhat related but *non*critical mechanism of slowly relaxing local structure[1,3] (SRLS) is likely to be more relevant. In the SRLS model the slowly fluctuating components of the anisotropic intermolecular potential are regarded as a local structure, which persists for a mean time τ_x much longer than the rotational correlation time τ_R. SRLS appears to be important in smectics.[2,26] It has also been suggested that the smaller probes such as PD-tempone are expelled from the aromatic region of the layered structure in the smectic phase.[2,27] In this case, SRLS may be associated with a dynamic cooperativity of solvent hydrocarbon chain motion[28] sensed by the probe molecule. That is, the probe undergoes rapid reorientation in the locally ordered hydrocarbon chain region of the mesophase, followed by much slower relaxation of the local order. In other studies it has been inferred that SRLS is important in nematics[29] and in isotropic phases of nematogenic molecules above the NI transition.[30]

NMR experiments to elucidate the details of molecular dynamics in liquid crystals are currently being utilized in many laboratories. Multifrequency NMR and field cycling NMR[16] are proving particularly useful. The potential of ESR in studies of liquid crystals has been realized to a much lesser extent, in part because of limitations of CW methods for spin–relaxation (see below). One reason why ESR can be very useful in such studies is the substantially lower magnetic fields required to polarize the electron spins. At the high magnetic fields typical of modern NMR spectrometers the liquid crystalline phases, characterized by molecules of substantial anisotropy in their diamagnetic susceptibility, align with the mesogen director parallel to the external field direction. Orientation dependent nuclear spin–relaxation measurements in the smectic A and C phases are thus difficult. Nevertheless some proton T_1 and $T_{1\rho}$ measurements,[18,19] as well as ^{2}H T_1 measurements[31] have been reported. As we will see in the following sections, such orientation dependent relaxation measurements can be routinely performed at the lower external magnetic fields of ESR, and in fact are found to be sensitive to the details of the molecular dynamics.

B. Modern ESR methods

In conventional ESR experiments, based upon continuous microwave irradiation, one deduces aspects of the reorientational process by simulating the spectral line shapes. In the motional narrowing regime one obtains several Lorentzian lines whose widths include contributions from the spectral densities of the motion at zero frequency, the hyperfine frequency ω_a, and the electron Larmor frequency ω_e.[1-3] We have previously pointed out that electron–electron double resonance (ELDOR) experiments[32-34] combined with ESR linewidth and saturation studies would, in principle, be very useful to decompose the electron spin–relaxation data into the specific spectral densities occuring at ω_e, ω_a, and $\omega = 0$.[4,34,35] The additional data from ELDOR would thereby permit a more critical test of the frequency dependence of

the spectral densities than could be obtained from just linewidth data. This was illustrated by van der Drift and Smidt who worked with a specially constructed CW ELDOR unit and completed such experiments on PD-tempone in isotropic media[36] and in the liquid crystalline solvent 8CB.[26] However, from an experimental point of view, the CW ELDOR technique, combined with CW linewidth and saturation suffer from possible systematic error due to effects of inhomogeneous broadening, although efforts are made to account for them.

We have recently developed several modern time domain ESR techniques for the study of spin–relaxation and motional dynamics. Our initial plan was to apply electron spin–echo (ESE) techniques to spin–relaxation in liquid crystals because it would offer: (1) the ability to separate homogeneous from inhomogeneous contributions to the linewidths; (2) the ease of simultaneously performing T_1 measurements; (3) the possibility that special ESE techniques could provide information on motional dynamics in addition to that from CW studies; and (4) the possibility of extending the range of study to slower motions.

When an echo technique is applied to spin–probes with inhomogeneously broadened CW ESR lines (e.g., due to unresolved—or partially resolved—proton super hf interactions in the case of nitroxides) the measured phase-memory time T_M is equal to T_2, the homogeneous linewidth of a single spin–packet.[37-39] Our past attempts at removing, or at least reducing, the inhomogeneous broadening were to utilize deuterated spin–probes such as PD-tempone for this purpose, but it is inconvenient to have to perdeuterate all the spin–probes and –labels. A more serious problem occurs in the case of oriented liquid crystalline samples, where small amounts of disorder can lead to inhomogeneous broadening that is difficult to distinguish from motional broadening.[2] In fact, we have shown that standard well-oriented tube samples typically exhibit some orientation dependent inhomogeneous line broadening from residual "mosaicity," especially in the smectic phases, and it is very difficult to reliably deconvolute it from the CW line shapes. Plate samples can also cause a variety of problems in CW ESR.[35]

In order to realize the potential of ESR relaxation studies, we have developed pulsed ELDOR techniques.[40-43] The most powerful of these is the two–dimensional Fourier transform ELDOR method (2D ELDOR).[40-42] This has advantages over CW ELDOR in that: (1) relaxation rates are directly measured rather than just their ratios; (2) the effects of inhomogeneous broadening are canceled out; (3) the radiation fields (as well as the field modulation) are absent during the main evolution time of the spins; and (4) *all* of the ELDOR transitions, as well as the ESR transitions, are *simultaneously* obtained in a single 2D spectrum. Thus, (1) removes the need for additional techniques; (2) suggests greater accuracy in data analysis (even without having to resort to deuteration of spin–labels); (3) eliminates complicating effects of finite irradiation fields in the analysis of the experiment; and (4) means greater efficiency in the data acquisition and greater reliability. Such a technique now enables us to distinguish in much greater detail, and with high reliability, the various spin relaxation processes and their

associated spectral densities for our studies.

The 2D ELDOR technique is first of all based upon Fourier transform (FT) ESR which was only very recently developed. This had posed a great instrumental challenge, but, because of new developments in microwave and digital electronics, it has been possible to obtain the broadband irradiation and detection required for ESR (~ 100 MHz for motionally narrowed nitroxides) at microwave frequencies, including the nanosecond time resolution required.[40,41]

In this paper we describe an extensive study of the dynamics of the nitroxide spin probe 2,2,6,6-tetramethyl-4-piperidone-N-oxyl-d_{16} (PD-tempone) in the smectic A phase of the liquid crystal mixture, S2 (cf. Fig. 1) performed by a combination of electron spin–echo T_2 measurements, and 2D ELDOR measurements. We also contrast these results with those obtained from CW ESR. These studies are performed as a function of both temperature and sample orientation in the magnetic field. We demonstrate the significant dependence of spin–relaxation on director orientation in smectics, and we utilize our orientation dependent data to investigate the relevance of several models of solute dynamics in the smectic mesophase.

II. THEORETICAL BACKGROUND

A. The smectic A phase

All nematic and smectic A phases have orientational order. That is, orientational order parameters $\langle \mathscr{D}_{KM}^{L}(\Omega)\rangle$ defined by

$$\langle \mathscr{D}_{KM}^{L}(\Omega)\rangle = \frac{1}{Z}\int d\Omega \exp[-U(\Omega)/kT]\mathscr{D}_{KM}^{L}(\Omega),$$
$$(1)$$

are nonzero, where Z is the normalization constant given by

$$Z = \int d\Omega \exp[-U(\Omega)/kT],\qquad (2)$$

$\mathscr{D}_{KM}^{L}(\Omega)$ are the Wigner rotation matrix elements and $U(\Omega)$ is the intermolecular potential. In the well known Maier–Saupe molecular (or mean) field description of uniaxial nematics[44] this potential is of the form $S\mathscr{D}_{00}^{2}(\Omega) = SP_2(\cos\beta)$, where the order parameter S is defined by $S \equiv \langle \mathscr{D}_{00}^{2}(\Omega)\rangle$. In the case of solute probe ordering Polnaszek and Freed define the potential $U(\Omega)$ as a potential of mean torque,[1,49] given in uniaxial phases by

$$U(\Omega) = \sum_{L=0,2,4}\left\{\epsilon_0^L\mathscr{D}_{00}^{L}(\Omega) + \sum_{0<K\leqslant L}\epsilon_{K\pm}^{L}\left[\mathscr{D}_{K0}^{L}(\Omega)\right.\right.$$

$$\left.\left.\pm \mathscr{D}_{-K0}^{L}(\Omega)\right]\right\}.\qquad (3)$$

The terms in Eq. (3) for which $K \neq 0$ arise from any lack of axial symmetry of the solute spin probe. For simplicity, one often only considers the leading term $\epsilon_0^2\mathscr{D}_{00}^{2}(\Omega)$ in Eq. (3), which has the angular dependence of the Maier–Saupe potential, but does not depend explicitly on S, since it is not a mean-field expression.

In the smectic phase, unlike in the nematic phase, there is also translational order, evidenced by the organization of

liquid crystal molecules into layers. The Maier and Saupe[44] description of the nematic phase was extended by McMillan[45] and Kobayashi[46] to describe the smectic A phase. McMillan introduced an additional order parameter to describe the positional ordering of the molecules in the layered structure of the smectic A phase. The Maier–Saupe and McMillan models have in common that the intermolecular potential may be replaced by a mean-field potential for a single molecule.[47] In the smectic A case this potential is also a periodic function of z/d, where z is associated with translation along the director and d is the bilayer thickness, i.e., $U = U(\Omega,z/d)$. Specifically, one can write the McMillan *form* for the mean-field potential as[48]

$$U(\beta,z/d) = U_0 + U_1\gamma\cos\left(\frac{2\pi z}{d}\right)$$

$$+ \left[W_0 S + W_1\sigma\cos\left(\frac{2\pi z}{d}\right)\right]P_2(\cos\beta),\quad (4)$$

where S, γ, and σ are the mean-field order parameters associated with orientation, position, and the coupling of orientation and position, respectively. More generally, one can utilize the functional *form* of Eq. (4) with respect to z and $\mathscr{D}_{00}^{2}(\Omega)$ as the leading term in an expansion of the "potential of mean force and torque" without invoking the mean-field approach in which U depends explicitly on the mean-field order parameters (cf. below).[7,49]

B. Spin–relaxation in the motional narrowing regime

Spin–relaxation in the motional narrowing regime is determined by the reduced correlation function

$$\langle \mathscr{H}_1(\Omega,t)\mathscr{H}_1^*(\Omega_0,t=0)\rangle - \langle \mathscr{H}_1(\Omega)\rangle\langle \mathscr{H}_1^*(\Omega_0)\rangle,\quad (5)$$

where $\mathscr{H}_1(\Omega)$ is the time dependent part of the spin–Hamiltonian given by[50]

$$\mathscr{H}_1(\Omega) = \sum_{L,K,M}(-1)^K\mathscr{D}_{-KM}^{L}(\Omega)F_{\mu}'^{(L,K)}A_{\mu}^{(L,M)},\qquad (6)$$

where the $F_{\mu}'^{(L,K)}$ and $A_{\mu}^{(L,M)}$ are irreducible tensor components of rank L, with F' in molecule-fixed coordinates, while A is a spin–operator in the laboratory axis system. The Euler angles $\Omega = (\alpha,\beta,\gamma)$ refer to the orientation of the principal axis system of the diffusion tensor (the molecule frame) with respect to the laboratory frame. More generally we have

$$\mathscr{H}_1(\Omega,\Psi) = \sum_{L,K,M,M'}(-1)^K\mathscr{D}_{-KM'}^{L}(\Omega)\mathscr{D}_{M',M}^{L}(\Psi)$$

$$\times F_{\mu}'^{(L,K)}A_{\mu}^{(L,M)},\qquad (7)$$

where the Euler angles $\Omega = (\alpha,\beta,\gamma)$ refer to the orientation of the molecular frame with respect to the director frame, whereas the Euler angles $\Psi = (0,\theta,\phi)$ denote the orientation of the director with respect to the laboratory frame. We assume for the time being that the angles Ψ are time independent so that Eqs. (5) and (6) apply. Since the time dependence of $\mathscr{H}_1(\Omega)$ is then carried entirely by the $\mathscr{D}_{-K,M}^{L}(\Omega)$, we need only consider the correlation functions of the $\mathscr{D}_{-K,M}^{L}(\Omega)$ given by

$$C_{-K,-K',M,M'}(t) = \langle \mathscr{D}_{K,M}^{(2)}(\Omega)\mathscr{D}_{K',M'}^{(2)*}(\Omega_0)\rangle$$
$$- \langle \mathscr{D}_{K,M}^{(2)}(\Omega)\rangle\langle \mathscr{D}_{K',M'}^{(2)*}(\Omega_0)\rangle. \quad (8)$$

The spectral densities are Fourier–Laplace transforms of the correlation functions of Eq. (8), i.e.,

$$j_{K,K',M,M'}(\omega) = \mathrm{Re}\int_0^\infty dt\, C_{K,K',M,M'}(t)e^{-i\omega t}\delta_{M,M'}, \quad (9)$$

where $\delta_{M,M'}$ appears because for a uniaxial phase $M = M'$. Although the fundamental spectral densities important for spin relaxation are indeed given by Eqs. (8) and (9), it is convenient to define spectral densities directly from Eqs. (5) and (6) for ease of relating to observables. Thus, we obtain the measurable spectral density

$$J_M^{\mu\nu}(\omega) = \sum_{K,K'} F_\mu^{'2,K}F_\nu^{'2,K'*}j_{K,K',M,M'}(\omega)\delta_{M,M'}, \quad (10)$$

where μ and ν indicate the magnetic tensors associated with the particular interactions.

In general the spectral densities of Eq. (9) are derived from a stochastic time evolution operator Γ via the resolvent

$$j_{K,K',M,M'}(\omega) = \mathrm{Re}\{\langle \delta D_{KM}^2|(i\omega + \Gamma)^{-1}|P_{eq}\delta D_{K'M'}^2\rangle\}, \quad (11)$$

where P_{eq} is the unique equilibrium probability distribution obeying the relation

$$\Gamma P_{eq} = 0 \quad (12)$$

and the bra $\langle \delta D_{KM}^2|$ is defined by

$$\langle \delta D_{KM}^2|\Omega\rangle \equiv D_{KM}^2(\Omega) - \langle D_{KM}^2(\Omega)\rangle. \quad (13)$$

Thus, δD_{KM}^2 denotes the deviation from the thermal average $\langle D_{KM}^2\rangle$. In the following sections the spectral densities are given explicitly or they are derived from a stochastic operator Γ utilizing Eq. (11).

For a single nuclear spin of I we have for the dependence of T_2 on the z component of nuclear spin M_I

$$T_2(M_I)^{-1} = A + BM_I + CM_I^2, \quad (14)$$

where[1]

$$A - A' = \frac{1}{3}I(I+1)\gamma_e^2\sum_{K,K'}D_KD_{-K'}\{j_{K,K',0}(\omega_e)$$
$$+ 3j_{K,K',1}(\omega_a) + 6j_{K,K',2}(\omega_e)\}$$
$$+ \frac{\hbar^2\gamma_e^2}{16\beta_e^2}\sum_{K,K'}F_KF_{-K'}\{4j_{K,K',0}(0)$$
$$+ 3j_{K,K',1}(\omega_e)\}, \quad (15)$$

$$B = -\frac{\hbar\gamma_e^2}{\sqrt{6}\beta_e}\sum_{K,K'}D_KF_{-K'}\{4j_{K,K',0}(0)$$
$$+ 3j_{K,K',1}(\omega_e)\}, \quad (16)$$

$$C = \frac{\gamma_e^2}{3}\sum_{K,K'}D_KD_{-K'}\{8j_{K,K',0}(0)$$
$$- j_{K,K',0}(\omega_e) + 6j_{K,K',1}(\omega_e)$$
$$- 3j_{K,K',1}(\omega_a) - 6j_{K,K',2}(\omega_e)\}, \quad (17)$$

where the D_K and F_K are the spherical tensor components of the electron–nuclear dipolar (END) and Zeeman tensors in the diffusion tensor principal axis system,[51] and where the $\omega_a = (1/2)a|\gamma_e| \pm \omega_n$, with ω_n the nuclear Larmor frequency. In the case of PD-tempone, the y axis of the magnetic tensor principal axis system is coincident with the z axis of the diffusion tensor principal axis system, and the probe is said to be "y ordered." In Eqs. (15)–(17) and below, we have removed the redundant M' subscript on the spectral densities. In terms of measurable spectral densities [cf. Eq. (10)] we obtain

$$A - A' = 2J_1^{DD}(\omega_a) + \tfrac{2}{3}J_0^{DD}(\omega_e) + 4J_2^{DD}(\omega_e)$$
$$+ \tfrac{8}{3}J_0^{GG}(0) + 2J_1^{GG}(\omega_e), \quad (18)$$

$$B = \tfrac{16}{3}J_0^{DG}(0) + 4J_1^{DG}(\omega_e), \quad (19)$$

$$C = \tfrac{8}{3}J_0^{DD}(0) - J_1^{DD}(\omega_a) + 2J_1^{DD}(\omega_e)$$
$$- \tfrac{1}{3}J_0^{DD}(\omega_e) - 2J_2^{DD}(\omega_e). \quad (20)$$

A' in Eqs. (15) and (18) includes all other nuclear-spin independent line-broadening mechanisms, which in the case of ESE T_2's is predominantly spin–rotation[1,4,51,52] for low concentrations of probe, whereas Heisenberg spin–exchange becomes important for higher concentrations.[34] For the nuclear spin–transition rate $2W_n$ we have

$$2W_n = J_1^{DD}(\omega_a) = \gamma_e^2\sum_{K,K'}D_KD_{-K'}j_{K,K',1}(\omega_a) \quad (21)$$

and for the terms involving electron spin–transitions we obtain[26,34]

$$W_e(M_I) = W_e^{SR} + 2J_1^{GG}(\omega_e)$$
$$+ 4J_1^{DG}(\omega_e)M_I + 2J_1^{DD}(\omega_e)M_I^2, \quad (22)$$

$$W_{x_1} = \tfrac{2}{3}J_0^{DD}(\omega_e), \quad (23)$$

$$W_{x_2} = 4J_2^{DD}(\omega_e), \quad (24)$$

where W_{x_1} and W_{x_2} are the cross-relaxation rates associated with $S_\pm I_\mp$ and $S_\pm I_\pm$, respectively.

Equations (15)–(24) are applicable when the director is aligned parallel to the magnetic field. If the director is tilted by an angle θ with respect to the magnetic field we replace the spectral densities in these equations by:

$$\hat{j}_{K,K',M}(\omega,\theta) = \sum_{M'=-2}^{+2}|d_{M,M'}^{(2)}(\omega)|^2 j_{K,K',M'}(\omega), \quad (25)$$

or alternatively

$$\hat{J}_M^{\mu\nu}(\omega,\theta) = \sum_{M'=-2}^{+2}|d_{M,M'}^{(2)}(\theta)|^2 J_{M'}^{\mu\nu}(\omega), \quad (26)$$

where the $d_{M,M'}^{(2)}(\theta)$ are the reduced Wigner rotation matrix elements of rank two, which can be evaluated in terms of their Clebsch–Gordon series expansions,[53]

$$|d_{MM'}^{(2)}(\theta)|^2 = (-1)^{M-M'}\sum_{l=0,2,4}C(2,2,l;M,-M)$$
$$\times C(2,2,l;M',-M')d_{00}^{(l)}(\theta). \quad (27)$$

The spectral densities in Eq. (26) have the property[1] that

$$J_M^{\mu\nu}(\omega) = J_{-M}^{\mu\nu}(\omega) \quad (28)$$

and hence the angular dependence of $\hat{J}_M^{\mu\nu}(\omega,\theta)$ is fully de-

scribed by the spectral densities $J_0^{\mu\nu}(\omega), J_1^{\mu\nu}(\omega)$, and $J_2^{\mu\nu}(\omega)$. In this version of the motional narrowing theory, the ^{14}N spin is assumed to be quantized along the laboratory z axis. Luckhurst and Zannoni[54] point out that the form of Eq. (26) is accurate only when the orientational ordering of the probe is weak (e.g., $S \leqslant 0.3$), such that the axis of ^{14}N spin quantization does not deviate substantially from the laboratory z axis. Thus we have for the orientation dependent W_n in the case of weak probe ordering

$$2W_n(\theta) = \tfrac{3}{2}\cos^2\theta \sin^2\theta \, J_0^{DD}(\omega_a)$$
$$+ \tfrac{1}{2}[(1 - 2\cos^2\theta)^2 + \cos^2\theta]J_1^{DD}(\omega_a)$$
$$+ \tfrac{1}{2}(1 - \cos^4\theta)J_2^{DD}(\omega_a) \qquad (29)$$

and in general we have

$$J_0(\omega,\theta) = \tfrac{1}{4}(1 - 3\cos^2\theta)^2 J_0(\omega) + 3\cos^2\theta \sin^2\theta \, J_1(\omega)$$
$$+ \tfrac{3}{4}\sin^4\theta \, J_2(\omega), \qquad (30)$$

$$J_1(\omega,\theta) = \tfrac{3}{2}\cos^2\theta \sin^2\theta \, J_0(\omega)$$
$$+ \tfrac{1}{2}[(1 - 2\cos^2\theta)^2 + \cos^2\theta]J_1(\omega)$$
$$+ \tfrac{1}{2}(1 - \cos^4\theta)J_2(\omega), \qquad (31)$$

$$J_2(\omega,\theta) = \tfrac{3}{8}\sin^4\theta \, J_0(\omega) + \tfrac{1}{2}(1 - \cos^4\theta)J_1(\omega)$$
$$+ \tfrac{1}{8}[(1 + \cos^2\theta) + 4\cos^2\theta]J_2(\omega). \qquad (32)$$

Thus, the orientation dependent spin relaxation rates such as the $W_n(\theta)$ yield with the application of Eqs. (30)–(32) the three spatial densities $J_0^{DD}(\omega), J_1^{DD}(\omega)$, and $J_2^{DD}(\omega)$. We will see in the following sections that an experimental determination of these three spectral densities allows for a much closer comparison of theoretical models of the dynamics with experiment than is possible without the orientation dependent data.

C. 2D ELDOR

The general theory for 2D ELDOR has been outlined previously.[41] In the case of nonnegligible Heisenberg exchange (ω_{HE}) and ^{14}N spin–relaxation (W_n) we obtain six equations in the two unknowns ω_{HE} and W_n from which to determine the two relaxation rates from the volumes of six 2D ELDOR cross peaks relative to the three autopeaks. A detailed examination of these expressions and their generalizations for nonnegligible nuclear–spin dependent nonsecular terms (e.g., cross relaxation) is given in Appendix A. In the special case where nuclear–spin dependent nonsecular terms as well as Heisenberg exchange are negligible, then only cross peaks for which $\Delta M_I = \pm 1$ are typically observed (with the $\Delta M = \pm 2$ cross peaks typically much weaker), and we obtain the very simple expression (in the notation of Ref. 41 and Appendix A)

$$6W_n = \frac{1}{T}\ln\left(\frac{2\widehat{Q}_{mj}V_j r_{2_j} + V_m r_{2_m}}{V_m r_{2_m} - \widehat{Q}_{mj}V_j r_{2_j}}\right), \qquad (33)$$

which applies to the two cross-peaks for which $m = \pm 1$ and $j = 0$, where T is the mixing time, $\widehat{Q}$ is the normalized matrix of 2D ELDOR peak volumes, and the products $V_i r_{2_i}$ are

determined from the peak areas obtained from a single microwave pulse experiment, (cf. Appendix A). Under these conditions, Eq. (33) enables a rapid determination of W_n directly from two of the four cross peaks obtained in the 2D ELDOR spectrum. [The other two cross peaks, i.e., $m = 0$, $j = \pm 1$, also provide information about W_n, but the expressions are somewhat more complicated than Eq. (33) (cf. Appendix A.)]

D. Anisotropic rotational diffusion and anisotropic viscosity

Anisotropic Brownian motion in the presence of a static orienting potential is described by the rotational analogue of the Smoluchowski equation.[55] The Smoluchowski operator is given by

$$\tilde{\Gamma}_\Omega = \mathbf{M}\cdot\mathbf{R}\cdot\mathbf{M} + [\mathbf{M}\cdot\mathbf{R}\cdot(\mathbf{M}U)]/2kT + \mathbf{T}\cdot\mathbf{R}\cdot\mathbf{T}/(2kT)^2, \qquad (34)$$

where $\mathbf{M}$ is the generator of infinitesimal rotations about the molecular axes and $\mathbf{R}$ is the diffusion tensor for the molecule and is diagonal in the molecular coordinate system.[2] Note that $\tilde{\Gamma}_\Omega$ is written in the symmetrized form obtained from Γ_Ω by the symmetrizing transformation[56]

$$\tilde{\Gamma}_\Omega = P_0^{-1/2}(\Omega)\Gamma_\Omega P_0^{1/2}(\Omega). \qquad (35)$$

The external torque $\mathbf{T}$ experienced by the molecule is related to the potential of mean torque $U(\Omega)$ by

$$\mathbf{T} = i\,\mathbf{M}U(\Omega). \qquad (36)$$

Polnaszek and Freed account for anisotropies in the viscosity of the solvent with the addition of a Smoluchowski operator to Eq. (34) which is diagonal in the laboratory coordinate system.[1] This operator may be obtained from Eq. (34) by replacement of $\mathbf{M}$ in Eqs. (34) and (36) with $\mathbf{N}$, the generator of infinitesimal rotations about the laboratory axes, and the replacement of $\mathbf{R}$ with a diffusion tensor $\hat{\mathbf{R}}$ whose principal axes coincide with the laboratory axes. Polnaszek and Freed did not consider a cross term between rotational diffusion (RD) and anisotropic viscosity (AV). Such a cross term may be important if the time scales for reorientation about the laboratory axes and the molecular axes are comparable. An expression applicable in the hydrodynamic limit has been derived by Moro and Nordio by relating the diffusion tensor to the anisotropic friction tensor via the Einstein relation.[57] The Polnaszek and Freed expression cannot be derived from hydrodynamic arguments, but merely models the effects of combined RD and AV with a diffusion operator separable into two parts: one diagonal in the molecular frame and one diagonal in the lab frame. Further aspects of combined RD and AV are considered by Lin and Freed.[2]

E. Order director fluctuations

Pincus suggested that fluctuations in the orientation of the director with respect to the magnetic field may be an important mechanism of spin–relaxation in nematics.[8] Doane et al. introduced the notion of a finite cutoff frequency of the Fourier modes used to characterize these fluctuations.[10] The amplitude of the mean square fluctuations of

the director for the qth mode and its decay time τ_α (**q**) have been derived by Schaetzing and Litster.[58] The presence of order director fluctuations (ODF) implies a time dependence of the Euler angles Ψ in Eq. (7), in addition to the usual time dependence of the Euler angles Ω. The combined effect of the time dependent Ω and Ψ on spin–relaxation in nematics has been considered by Ukleja et al.[9] and by Freed.[3] Freed obtains the following expression for the spectral densities applicable in the nematic phase:

$$j_{K,M}(\omega) = \frac{\kappa(K,M)\tau_R}{1+\omega^2\tau_R^2}$$
$$+ \frac{3}{2}S^2\mathscr{A}\delta_{K,0}\delta_{M,\pm 1}\left[\sqrt{\frac{\pi}{2}}\frac{u(\omega/\omega_c)}{\sqrt{\omega}}\right.$$
$$\left. - \left(\frac{\tau_R}{1+\omega^2\tau_R^2}\right)\frac{2}{\sqrt{\pi}}\omega_c^{1/2}\right], \qquad (37)$$

where[1,10]

$$u(\omega/\omega_c) = 1 - \frac{1}{2\pi}\ln\left|\frac{1+\sqrt{2\omega/\omega_c}+\omega/\omega_c}{1-\sqrt{2\omega/\omega_c}+\omega/\omega_c}\right|$$
$$- \left(\frac{1}{\pi}\tan^{-1}\frac{\sqrt{2\omega/\omega_c}}{1-\omega/\omega_c}+\rho\right),$$

$$\rho = \begin{cases}0 & \omega/\omega_c < 1 \\ 1 & \omega/\omega_c > 1\end{cases} \qquad (38)$$

and where $S = \langle\mathscr{D}_{00}^2(\Omega)\rangle$ is the orientational order parameter defined in Eq. (1). In Eq. (38) ω_c is the cutoff frequency given by $\omega_c = Kq_c^2/\eta$ that is introduced because the hydrodynamic theory should break down for wavelengths $\lambda_c = 2\pi/\omega_c$ comparable to molecular dimensions, with K the average elastic constant [involving splay (K_1), twist (K_2), and bend (K_3) deformations[47]] in the one constant approximation, and η the average viscosity. We define the cutoff wave vector q_c by $q_c = 2\pi/l$, where l is a molecular dimension; Zientara and Freed present a more detailed theoretical discussion of the hydrodynamic cutoff wave vector.[59] Also in Eq. (38) $\kappa(K,M)$ is the correlation function for anisotropic rotational diffusion and $\mathscr{A}$ is defined as $\mathscr{A} = k_B T_\eta^{1/2}/2\pi^{3/2}K^{3/2}$. Thus for small ω/ω_c, $j_{0,\pm 1}(\omega)\sim\omega^{-1/2}$. For large ω/ω_c, $u(\omega/\omega_c)\to 0$ and the ODF spectral densities are suppressed, hence the choice of cutoff frequency is crucial in determining the importance of ODF to the spin–relaxation for large ω. Assuming typical values for a nematic of $K = 1.0\times 10^{-6}$ dyn, $\eta = 0.5$ P, and $l = 30\times 10^{-8}$ cm, we obtain for the cutoff frequency $\omega_c = 8.8\times 10^8$ s^{-1} or about 140 MHz. The difference between the Ukleja et al. treatment and the Freed treatment is that the former did not properly formulate the ODF/anisotropic diffusion cross term. The result is that the Ukleja et al. cross term remains nonzero even as the orientational order parameter (and hence the ODF) goes to zero in the isotropic limit, and is of the wrong sign. Recent NMR results have been fit successfully with the Freed formulas including the cross term but are inconsistent with the Ukleja et al. cross term.[60]

To obtain an expression for the order parameter from hf splittings the usual expression $S = \langle\mathscr{D}_{00}^2(\Omega)\rangle_\Omega$ is renormalized with respect to director fluctuations giving[3]

$$\widetilde{S} = \langle\mathscr{D}_{00}^2(\Omega)\rangle_{\Omega,\Psi}$$
$$\simeq \int d\Omega\int d\Psi f_{eq}(\Psi)P_{eq,\Psi}(\Omega)\mathscr{D}_{00}^2(\Omega), \qquad (39)$$

where $f_{eq}(\Psi)$ is the equilibrium probability distribution function for the director fluctuations and $P_{eq,\Psi}(\Omega)$ is the probability distribution in orientation Ω for an arbitrary value of the director Ψ. Plomp and Bulthuis[61] obtain the expression relating $\widetilde{S}$ to S in the lowest order approximation

$$\widetilde{S}\simeq S\{1-3/2\langle|\Theta|^2\rangle_\Psi\}, \qquad (40)$$

where $\langle|\Theta|^2\rangle_\Psi$ is the mean-squared amplitude of the ODF and is proportional to $\omega_c^{1/2}$. A similar treatment may be found in the work of Warner.[62] Thus, the nematic order parameter obtained from the hf splittings is to lowest order expected to be less than the actual orientational order parameter S.

The expressions for smectic ODF are complicated by the coupling of ODF modes to the (complex) smectic order parameter[63] $\psi = |\psi|e^{i\phi}$, and the absence of elastic deformations whose wavelengths exceed the dimension of a uniformly oriented domain. A proper theoretical account of smectic ODF may be found in the work of Vilfan et al.[18] Although they find a marked deviation from nematic-like behavior in both the frequency dependence of T_1 and the orientation dependence of $T_{1\rho}$, the orientation dependence of T_1 does not deviate in form from what is predicted by Eq. (37) and the ODF are suppressed at wave vectors beyond the cutoff q_c. Assuming an average viscosity[64] $\eta = 100$ P, an average elastic constant $K = 1.0\times 10^{-5}$ dyn, and $d = 30\times 10^{-8}$ cm, where d is the bilayer thickness, we obtain $\omega_c = 4.4\times 10^7$ s^{-1} or about 7 MHz, with ω_c defined as in Eqs. (37) and (38). Note that the smectic ODF cutoff is substantially lower than that obtained in the nematic phase. The smectic ODF measurements of Mugele et al.[12] suggest a substantially lower cutoff wave vector q_c consistent with a length of about 3×10^{-6} cm below which the hydrodynamic theory should break down.

F. Slowly relaxing local structure

Freed and co-workers[1-3] developed a model of slowly relaxing local structure or SRLS, to explain some anomalies in ESR line shape data. SRLS is characterized by the presence of a local order tensor

$$Q_{\alpha\beta} = \tfrac{1}{2}S_l(3n_\alpha n_\beta - \delta_{\alpha,\beta}), \qquad (41)$$

where $\hat{n}$ is the instantaneous director whose components n_α, n_β are referred to the lab z axis and S_l is the local order parameter. Alternately in irreducible tensor notation we have[3]

$$Q_M = S_l\mathscr{D}_{0,M}^2(\Psi) \qquad (42)$$

and local order parameter fluctuations described by the correlation function

$$C_{-K,M,-K',M'}(t) = S_l^2\langle\delta D_{0,M'}^{2*}(\Psi_0)\delta D_{0,M}^2(\Psi)\rangle\delta_{K,0}\delta_{K',0}, \qquad (43)$$

In this expression the local order parameter S_l is assumed

static. If we do not assume S_l remains constant, then it must be replaced by the mean square value $\langle |S_l|^2 \rangle$.[3] On a short time scale the probe dynamics is governed by simple anisotropic rotational diffusion in the presence or absence of an orienting potential. On a longer time scale the local structure relaxes according to the correlation function of Eq. (43). Hence the slowly fluctuating components of the anisotropic intermolecular potential are regarded as a local structure. The Freed derivation assumed that the $D_{0,M}^2(\Psi)$ relax isotropically with correlation time $\tau_x \gg \tau_R$ and hence

$$\langle \delta D_{0,M'}^{2*}(\Psi_0) \delta D_{0,M}^2(\Psi) \rangle = e^{-t/\tau_x} \delta_{M,M'}. \tag{44}$$

Upon incorporating the effects of a static orienting potential one obtains for axially symmetric ordering[3]

$$j_{KM}(\omega) = \frac{\kappa(K,M)\tau_R}{1 + \omega^2\tau_R^2} + \frac{1}{5} [5\kappa(0,M)]^2 \delta_{K,0} \langle |S_l|^2 \rangle$$

$$\times \left[\frac{\tau_x}{1 + \omega^2\tau_x^2} - \frac{\tau_R'}{1 + \omega^2\tau_R'^2} \right], \tag{45}$$

where $\tau_R'^{-1} \equiv \tau_R^{-1} + \tau_x^{-1} \cong \tau_R^{-1}$. The generalization of Eq. (45) to nonaxial molecular ordering may be found in Lin and Freed.[2] They also point out[1] that the τ_x modes may in general be M dependent, i.e., that the correlation function of Eq. (43) need not be a single exponential decay. Van der Drift and Smidt suggest that this M dependence may be considered due to anisotropic viscosity of the liquid crystalline medium.[26] These authors have observed deviations from a linear dependence of PD-tempone τ_R on η/T in several nematics using CW ESR and have attributed these observations to the presence of a local structure giving rise to a SRLS effect.[26] Nishida et al. have made analogous measurements using ^{2}H and ^{14}N NMR and have obtained good fits to the data with a SRLS model.[65] It is important to note that the local structure may persist and thus the local order parameter S_l may be nonzero even as $S \to 0$, i.e., in the isotropic limit. Zager and Freed[66] considered such a model in interpreting anomalies in CW linewidth parameters for PD-tempone in several isotropic solvents. When the orientational order parameter is nonzero, S must be renormalized as for ODF to obtain the measurable order parameter $\bar{S}$. In the SRLS case an expression analogous to Eq. (40) would be obtained, but with $\langle |\Theta|^2 \rangle$ replaced with $\langle |S_l|^2 \rangle$.

G. Rototranslational diffusion

Moro and Nordio have solved the diffusion equation for solutes in smectic phases subjected to a McMillan-type potential[7] (cf. Sec. II A). They write for the diffusion operator

$$\Gamma = \mathbf{M} \cdot \mathbf{R} \cdot P \mathbf{M} P^{-1} - \nabla \cdot \mathbf{D}^T \cdot P \nabla P^{-1}, \tag{46}$$

where P is shorthand for $P(\mathbf{r},\Omega)$ defined by

$$P(\mathbf{r},\Omega) = \exp[-U(\mathbf{r},\Omega)/kT], \tag{47}$$

∇ is the gradient operator referred to the laboratory frame, and $\mathbf{D}^T$ is the translational diffusion tensor. The potential used by Moro and Nordio in this model is given by

$$U(\beta,z/d)/kT = \{A + B\cos(2\pi z/d)\}\mathscr{D}_{00}^2(\beta)$$

$$+ C\cos(2\pi z/d), \tag{48}$$

where the angle β is obtained from $\Omega = (0,\beta,0)$ and z is associated with translation along the smectic director $\hat{n}$. There are thus three order parameters associated with the three potential parameters A, B, and C of Eq. (48); they are, respectively,

$$S = \langle \mathscr{D}_{00}^2(\beta) \rangle, \tag{49}$$

$$\sigma = \langle \cos(2\pi z/d)\mathscr{D}_{00}^2(\beta) \rangle, \tag{50}$$

$$\gamma = \langle \cos(2\pi z/d) \rangle. \tag{51}$$

Note that this potential has the symmetry of the McMillan potential [cf. Eq. (4)]. However, the parameters A, B, and C in Eq. (48) do not represent the mean-field quantities appearing in McMillan's expression. The Moro–Nordio form for the potential is rather a combination of a potential of mean torque and a potential of mean force, as well as a cross term. The Moro and Nordio treatment of solute diffusion in smectics is hence a logical extension of the theory for solute anisotropic diffusion in nematics. A generalization of this expression to apply both to fluctuations at the NA transition[5] and to rotational–translation coupling deep in the smectic phase has been proposed by Freed.[6]

There are several important implications of the potential of Eq. (48). The Moro and Nordio form for the potential accounts for the existence of translational order, which vanishes in the nematic and isotropic phases, and of orientational order, which persists throughout the smectic and nematic phases and vanishes in the isotropic phase. As a result of the coupling between orientation and position, the orientational order parameter is nonuniform across the smectic bilayer. Thus, the z-dependent local orientational order can be substantially larger for the probe located in the aromatic core region vs the more isotropic hydrocarbon region of the bilayer. That is, $P(\beta,z/d)$ defined by Eqs. (47) and (48) indicates a nonuniform distribution of probe along the smectic director, consistent with the observed preferential location of PD-tempone in the hydrocarbon region of several smectics.[2] Also important is the effect of translational diffusion of the probe parallel to the z direction. This motion has the effect of modulating the intensity of the orientational pseudopotential acting on the probe, and hence influencing the rotational motions. Typically, the rotational reorientation is more rapid than the translational diffusion across the bilayer. This mechanism of spin–relaxation is analogous to SRLS (cf. Sec. II F) in that rotational diffusion governs the short time behavior whereas relaxation of the local structure, resulting in this case from translation of the probe molecule, governs the longer time behavior. It is distinct from SRLS in that it requires solute diffusion to produce a modulation of S, the orientational order parameter, as opposed to local order fluctuations of the solvent. That is, SRLS does not necessarily require translational diffusion to produce the modulation.

The spectral densities appropriate for NMR and ESR are obtained numerically from the matrix representation of the diffusion operator Eq. (46) in a truncated basis of product functions

$$\Psi_{jpq,m} = \exp(2\pi miz/d)\mathscr{D}_{pq}^j(\alpha,\beta,\gamma), \tag{52}$$

where the notation of Ref. 7 is used for the Wigner functions in which q and p refer to body-fixed and space-fixed axes, respectively. Spectral densities defined in Eq. (11) are obtained with the use of the Lanczos algorithm by the method of Moro and Freed.[67] An important manifestation of translational order and translational diffusion in this model is a substantial enhancement at low-frequency of certain spectral densities in comparison with those obtained from the pure rotational Smoluchowski operator given in Eq. (34). In particular, only those spectral densities associated with the $\mathscr{D}_{KM}^{L}$ whose orientational average is nonzero are modified by translation. In the present case this means that the only self-correlation function that is modified by translation is $\langle \mathscr{D}_{00}^{2}(\Omega)\mathscr{D}_{00}^{2*}(\Omega_{0})\rangle$. This results from the fact that probe reorientation occurs much more rapidly than translation, such that at any given z a full orientational average is achieved.

III. EXPERIMENTAL

A. Sample preparation

The liquid crystal S2 is a eutectic mixture of three cyanobiphenyls: 4-cyano-4'-n-octyl biphenyl (8CB, 50%); 4-cyano-4'-n-decyl biphenyl (10CB, 39%); 4-cyano-4'-n-decyloxy biphenyl (10OCB, 11%). S2 was purchased from BDH Chemicals and used without further purification. The structures of the three component molecules are shown in Fig. 1. The nitroxide free radical 2,2,6,6-tetramethyl-4-piperidone-N-oxyl-d_{16} (PD-tempone) was synthesized by E. Igner and is shown in Fig. 2. Differential scanning calorimetry (DSC) indicated two phase transitions in the neat S2 over the temperature range 0–50 °C: one at 45.99 °C (NA) and the other at 47.65 °C (NI). The transition temperatures were found to be invariant with spin probe concentration over the range 0–2 × 10^{-3} M. Solutions of PD-tempone in S2
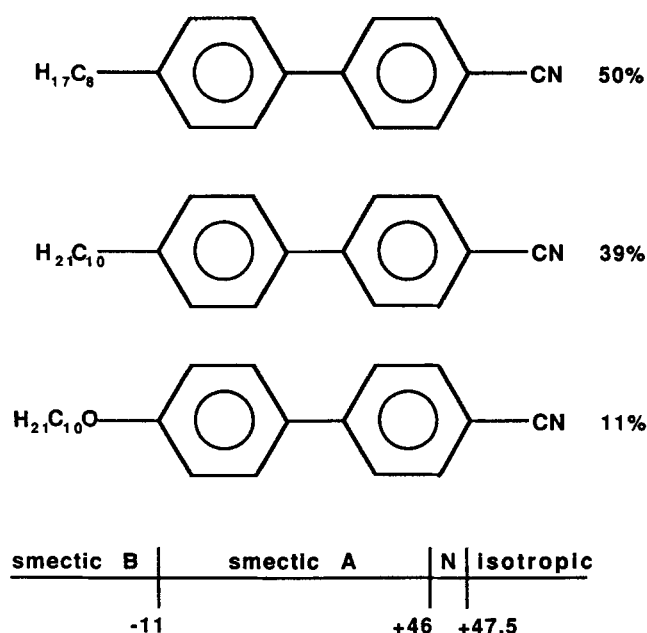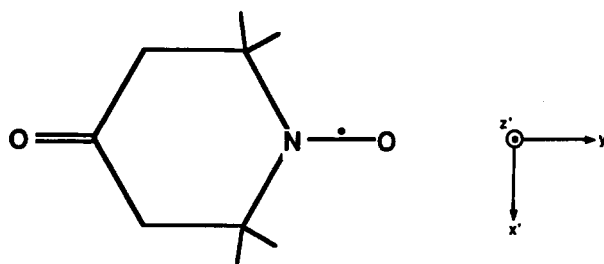

FIG. 2. Perdeuterated 2,2,6,6-tetramethyl-4-piperidone N-oxide (PD-tempone) showing the principal axis system for the magnetic tensors.

were prepared by stirring the mixtures overnight with the temperature maintained just above the nematic-isotropic phase transition. Solutions were transferred to 3 mm o.d. glass sample tubes or 8 mm o.d. glass NMR tubes and deoxygenated with at least four freeze/thaw cycles. Sample tubes were sealed under a vacuum and the samples were aligned in the 2 T magnetic field of a Jeol 90 NMR spectrometer.

B. Pulsed ESR spectrometer

Pulsed ESR measurements were performed on the home-built 2D Fourier transform ESR spectrometer described previously.[41] CW ESR linewidth measurements were performed on a Varian E-12 spectrometer using 10 kHz field modulation. Orientation dependent relaxation measurements were performed with 3 mm sample tubes mounted on a goniometer. The temperature in the active region of the cavity was controlled with a home-built fluid-flow system consisting of a mineral oil reservoir regulated by a NES-LAB RTE-210 constant temperature circulator. The temperature was monitored with a copper–constantan thermocouple placed just below the active region of the cavity within the mineral oil reservoir and referenced to an ice/water mixture. The thermoelectric voltage was measured with a Hewlett–Packard 3457A digital multimeter after calibration with a Hewlett–Packard platinum resistance thermometer.

C. CW ESR measurements

Homogeneous linewidths were obtained from the inhomogeneously broadened CW ESR lineshapes by an iterative method described earlier.[2] This method is based on the assumption that the only significant source of inhomogeneous broadening is super hf structure associated with the methyl deuterons of the PD-tempone spin–probe. The experimental line shape is compared to a theoretical line shape calculated using an estimated intrinsic derivative peak-to-peak width and hf splitting constant for the deuterons. An iterative procedure yields the intrinsic derivative peak-to-peak width: $2|\gamma_{e}|T_{2}^{-1}(3)^{-1/2}$ from which T_{2} is easily obtained. PD-tempone magnetic parameters were obtained from Lin and Freed[2] for the smectic A phase of 8CB and modified in accordance with the observed isotropic hf splittings[66] for S2 yielding $g_{xx} = 2.0092$, $g_{yy} = 2.0057$, $g_{zz} = 2.0016$, $A_{zz} = 5.57$ G, $A_{yy} = 4.98$ G, $A_{zz} = 33.47$ G.

smectic B | smectic A | N | Isotropic
-11 | +46 | +47.5

FIG. 1. Composition of the liquid crystal S2.

D. Electron spin–echo measurements

Electron spin–echo (ESE) measurements were performed with a ferromagnetic metallic object placed between the magnet pole faces in order to reduce the dc magnetic field homogeneity. Homogeneity reduction was necessary in these experiments in order to eliminate FID components following the second pulse of the $\pi/2$–τ–π–τ Hahn echo pulse sequence or the third pulse of the $\pi/2$–τ–$\pi/2$–T–$\pi/2 - \tau$ stimulated echo sequence. The T_2 for each hf line was obtained from the τ dependence of the Hahn echo amplitude by nonlinear least-squares parameter estimation. Estimates of W_n, ω_{HE}, and W_e were likewise obtained from the T dependence of the stimulated echo amplitude.

E. 2D ELDOR measurements

Electron–electron double resonance measurements were performed on 2.05×10^{-3} M PD-tempone in S2 by the 2D ELDOR method described previously.[40,41] Details of the experiment and a sample 2D ELDOR spectrum are shown in Fig. 3 and its caption. Heisenberg exchange was found to be unimportant, as established by the absence of any significant $\Delta M_I = \pm 2$ 2D ELDOR cross peaks (cf. Fig. 4) over the entire temperature range investigated, irrespective of director tilt.[42(b)] [This contrasts with our previous 2D ELDOR study of PD-tempone(1×10^{-3} M) in the much less viscous solvent toluene, where the predominent exchange mechanism is Heisenberg exchange as demonstrated by the fact that the $\Delta M_I = \pm 2$ cross peaks are comparable to the $\Delta M_I = \pm 1$ cross peaks[41].] The present results are consistent with CW linewidth measurements of Heisenberg exchange for PD-tempone in the smectic A phase of a mixture of related oxycyanobiphenyl based liquid crystals.[23]

Volume integrals of the pure absorption 2D Lorentzian line shapes were obtained from the 2D ELDOR spectra with the application of the 2D LPSVD method previously described.[42] The ^{14}N spin–relaxation rate $2W_n$ was derived from the 2D ELDOR volume integrals with the application of Eq. (33). Nuclear–spin dependent nonsecular terms could be neglected (see below). 2D ELDOR spectra at three different mixing times were collected at each temperature for the 0° and 90° director tilt experiments to facilitate statistical analysis. Orientation dependent experiments were performed at seven temperatures and typically involved seven tilt angles in the range 0°–90° and one mixing time. Sample rotations were achieved with a goniometer mount and any offset of the actual sample orientation from the intended orientation was corrected by fitting the observed orientation dependent hf splittings to the expression[2]

$$\langle a \rangle \simeq a_N + \tfrac{1}{2}\chi(3\cos^2\theta - 1). \tag{53}$$

F. Computation

Spectral densities were calculated from analytical expressions or were obtained numerically from the stochastic time evolution operator Γ utilizing Eq. (11). Linewidths and W_n's from the model of anisotropic viscosity were computed with slow-motional ESR line shape programs. All computations were performed on a Sun Microsystems 3/60 workstation.

IV. RESULTS AND DISCUSSION

A. Electron spin transitions

W_e was determined from the time evolution of the stimulated echo (SE) amplitude (cf. Appendix A and Table IV).
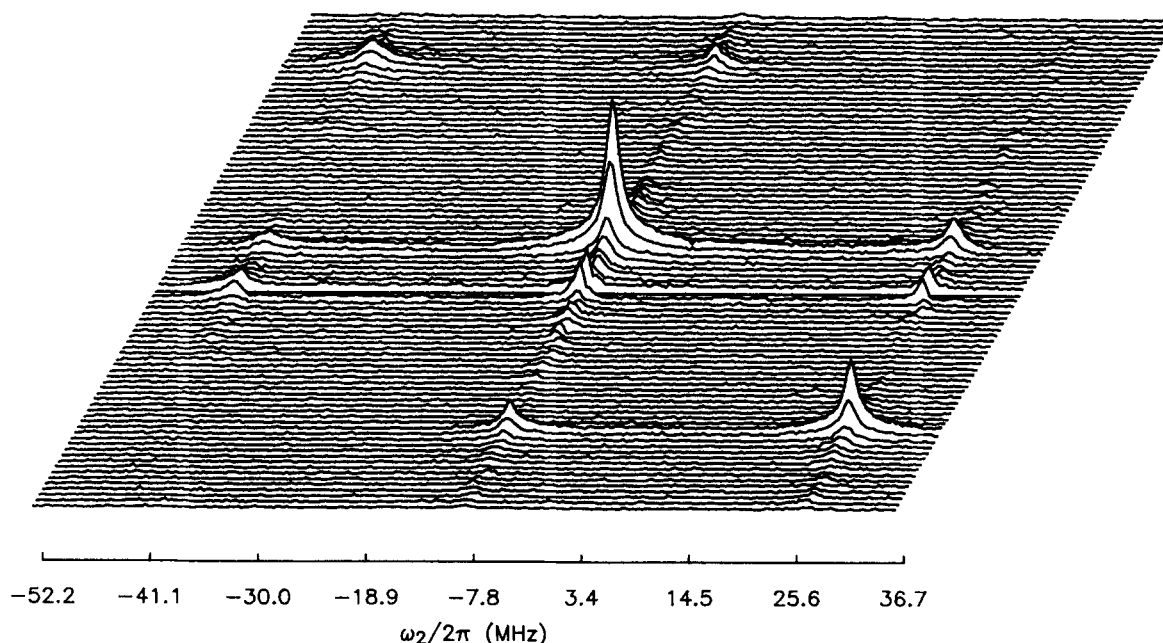

-52.2   -41.1   -30.0   -18.9   -7.8   3.4   14.5   25.6   36.7

$\omega_2/2\pi$ (MHz)

FIG. 3. Absolute value 2D ELDOR spectrum of 2.05×10^{-3} M PD-tempone in S2 at 35.5 ± 0.5 °C obtained with the smectic director aligned parallel to B_0; $t_p = 12$ ns; $\Delta t_1 = 7$ ns; $\Delta t_2 = 5.86$ ns; 128 samplings in t_1; eight step phase alternation sequence with 128 averages per step; dead time in t_1 of 66 ns; dead time in t_2 of 145 ns; mixing time $T = 5.48 \times 10^{-7}$ s; 256 complex data points per FID extending to 1.5 μs; acquisition time 51 min.
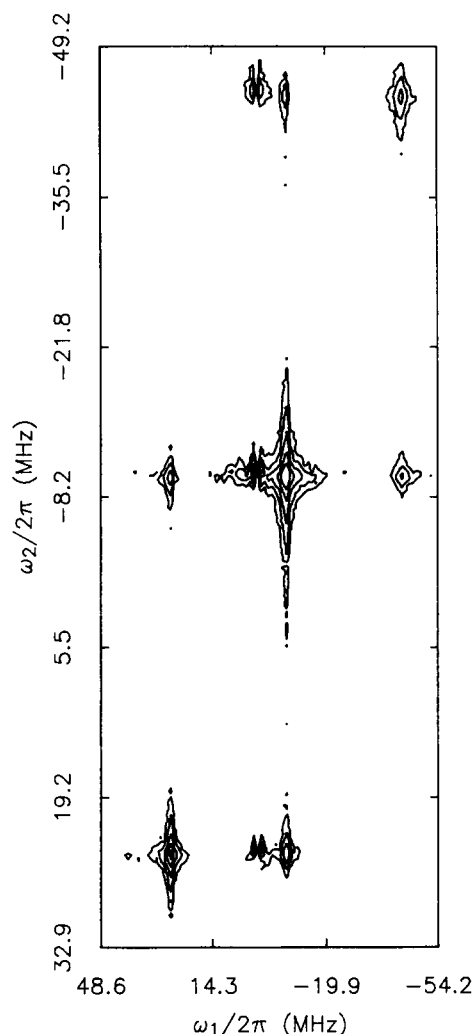
FIG. 4. 2D ELDOR contour map of the spectrum of Fig. 3. Note that absence of cross peaks connecting the two outer hf lines, indicative of a ^{14}N spin–relaxation mechanism.

The W_e's obtained for 2.0×10^{-3} M PD-tempone in S2 at 22 °C from SE(+ 1) and SE(0) (where the value in the parentheses gives the M_I of the hyperfine line studied) at 0° tilt are $4.57 \pm 0.04\times10^5$ and $4.58 \pm 0.05\times10^5$ s^{-1}, respectively, and from SE(+ 1) at 90° tilt $W_e = 3.82 \pm 0.03\times10^5$ s^{-1} thereby indicating some angular dependence to W_e. Nuclear spin dependent nonsecular terms were neglected in the analysis, so that one obtains a sum of either two or three exponentials, depending on the hf component, which include effects of W_n, ω_{HE}, and W_e.[68–70] [The W_n and ω_{HE} obtained from SE(+ 1) and SE(0) at 0° tilt are $2W_n = 0.89 \pm 0.16\times10^6$ s^{-1}, $\omega_{HE} = -0.01\pm0.18\times10^6$ s^{-1}; and $2W_n = 1.12 \pm 0.04\times10^6$ s^{-1} (if ω_{HE} is set to zero), respectively, and from SE(+ 1) at 90° tilt $2W_n = 1.18 \pm 0.12\times10^6$ s^{-1}, and $\omega_{HE} = -0.09 \pm 0.14\times10^6$ s^{-1}. These values are in agreement with 2D ELDOR (cf. below), and they show that W_n is substantial, whereas ω_{HE} is negligible.]

The neglect of nuclear spin dependent nonsecular terms is supported by our observed agreement between the SE and 2D ELDOR methods of determining W_n and ω_{HE}, since they are based upon different methods of analysis, and there-

fore should be differently affected if the neglect of these nonsecular terms were unjustified. We shall also show later in Sec. IV, that the fits of our data to appropriate models of molecular dynamics provide *a postieri* justification, because they lead to the prediction that such terms are too small to be observed experimentally.

On the other hand, in a general sense, we wish to point out that the equality of the W_e's obtained from the SE(+ 1) and SE(0) would be insufficient, in itself, to unequivocally demonstrate that nuclear spin dependent nonsecular terms are unimportant. After all, if they were important, then the analysis of the SE experiment should be regarded as a force fit of the signal to a sum of two or three exponentials when, in fact, there are five due to the five normal modes which are linear combinations of $W_e(+ 1)$, $W_e(0)$, and $W_e(- 1)$, as well as W_n, ω_{HE}, W_{x_1}, and W_{x_2} [70] [cf. Eqs. (22)–(24) and Appendix A). Thus, the simplified analysis imposes the constraint $W_e(+ 1) = W_e(- 1) = W_e(0) \equiv W_e$ rather than demonstrating it. (It would seem unreasonable to expect to accurately measure the effects of the sum of five exponential decays from each SE). Also in a general sense, we wish to point out that 2D ELDOR is less susceptible to model-dependent problems with the analysis as discussed more fully in Appendix A, and our experience has shown it to be more reliable than SE in extracting values of W_n even when the simplified analysis, in which the neglect of nuclear spin dependent nonsecular terms, is justified as in the present work.

B. Temperature-dependent relaxation

Using standard CW methods we obtained the orientational order parameter S as a function of temperature for cholestane spin–probe (CSL) in S2. The orientational order parameter of PD-tempone in S2 was determined from the hf splittings obtained by Fourier transformation of the FID's. The CSL molecule is known to report on the overall or "backbone" ordering of the liquid–crystalline phase.[24,28,35,71,72] Temperature-dependent orientational order parameters for CSL and PD-tempone in S2 are illustrated in Fig. 5. As expected, the CSL order parameter is substantially greater than that of PD-tempone throughout the smectic A and nematic phases.

Figure 6 illustrates the temperature dependent[14] N relaxation rates $2W_n$ of 2.0×10^{-3} M PD-tempone in S2 obtained for tilt angles of 0° and 90°. From the 0° tilt angle measurements we obtain the dipolar spectral densities $J_1^{DD}(\omega_a)$, whereas from $2W_n$ at 90° tilt we obtain the mean of $J_1^{DD}(\omega_a)$ and $J_2^{DD}(\omega_a)$. A nearly linear dependence of $\ln 2W_n$ on $10^3/T$ is obtained if one neglects the data very near the smectic A–nematic (NA) phase transition, where there is a substantial deviation from linearity. In the linear region (below 42.3 °C) we obtain for 0° tilt an Arrhenius activation energy $E_a = 10.49 \pm 0.79$ kcal mol^{-1} and for 90° tilt, $E_a = 10.60 \pm 0.72$ kcal mol^{-1}. The deviation from linearity as one approaches the NA transition is due in part to the reduction in orientational order. Quasicritical fluctuations may also be significant in this region,[3,5] but we have not pursued this matter further in the present work.

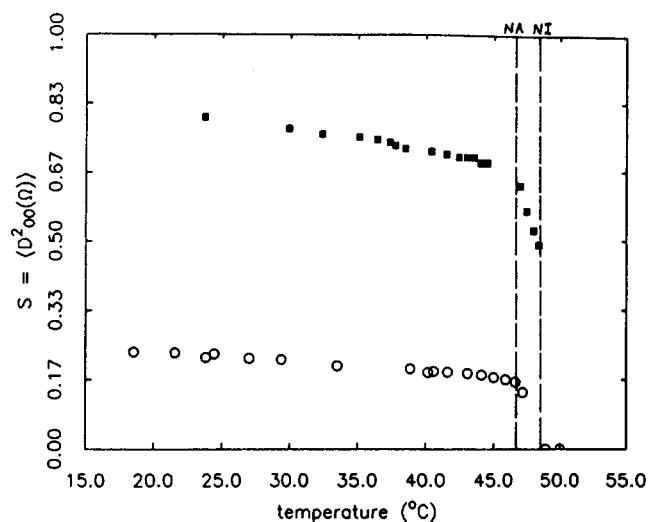Figure 7 illustrates the $T_2(M_I)$ obtained by electron

FIG. 5. Orientational order parameters for cholestane (solid boxes) and PD-tempone (open circles) in S2. Dashed lines indicate the locations of nematic–smectic A (NA) and nematic–isotropic (NI) phase transitions.
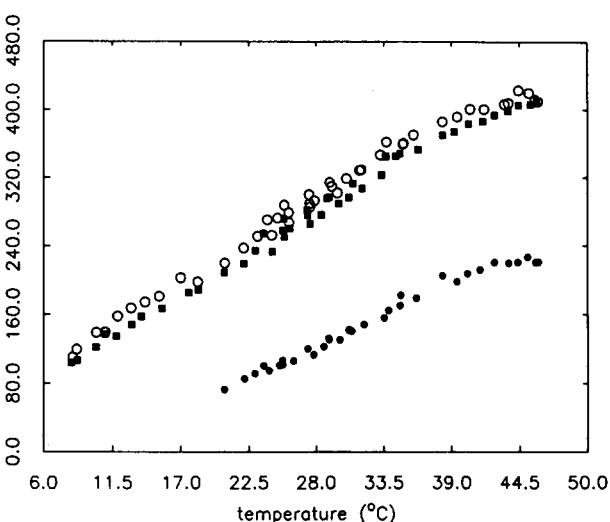

FIG. 7. Electron spin–echo T_2's of PD-tempone in S2: $M_I = +1$ (open circles); $M_I = 0$ (solid boxes); $M_I = -1$ (solid circles).

spin–echoes as a function of temperature in the smectic A, nematic, and isotropic phases of S2. The linewidth parameters A, B, and C were obtained from the electron spin–echo T_2's with the application of Eq. (14). In the absence of nuclear spin dependent nonsecular terms the Zeeman–dipolar spectral densities $J_0^{DG}(0)$ may be obtained directly from the T_2's and the dipolar spectral densities $J_0^{DD}(0)$ may be obtained from a combination of T_2 and ELDOR measurements via the expressions

FIG. 6. ^{14}N relaxation rate $2W_n$ of 2.0×10^{-3} M PD-tempone in S2: (a) $\hat{n} \| B_0$; (b) $\hat{n} \perp B_0$.

$$J_0^{DG}(0) = \frac{3}{16} B \qquad (54)$$

and

$$J_0^{DD}(0) = \frac{3}{8} (C + 2W_n). \qquad (55)$$

In Fig. 8 we illustrate the temperature dependence of $J_0^{DG}(0)$ and $J_0^{DD}(0)$. We obtain for $-J_0^{DG}(0)$ over the temperature range 20.5–42.3 °C an Arrhenius activation energy $E_a = 12.46 \pm 0.37$ kcal mol^{-1} with a preexponential factor $A = 4.83 \times 10^{-4}$ s^{-1}, whereas for $J_0^{DD}(0)$, $E_a = 12.40 \pm 0.38$ kcal mol^{-1} and $A = 1.32 \times 10^{-3}$ s^{-1}. The ratio $-J_0^{DG}(0)/J_0^{DD}(0)$ is nearly constant over this temperature range at a value of 0.40. This ratio is indicative of a smaller g tensor than END tensor contribution to $\langle |\mathcal{H}_1(\Omega)|^2 \rangle$. The ratio $J_0^{DD}(0)/J_1^{DD}(\omega_a)$ is about two at 20.5 °C and decreases to slightly greater than one near the NA transition.[73]
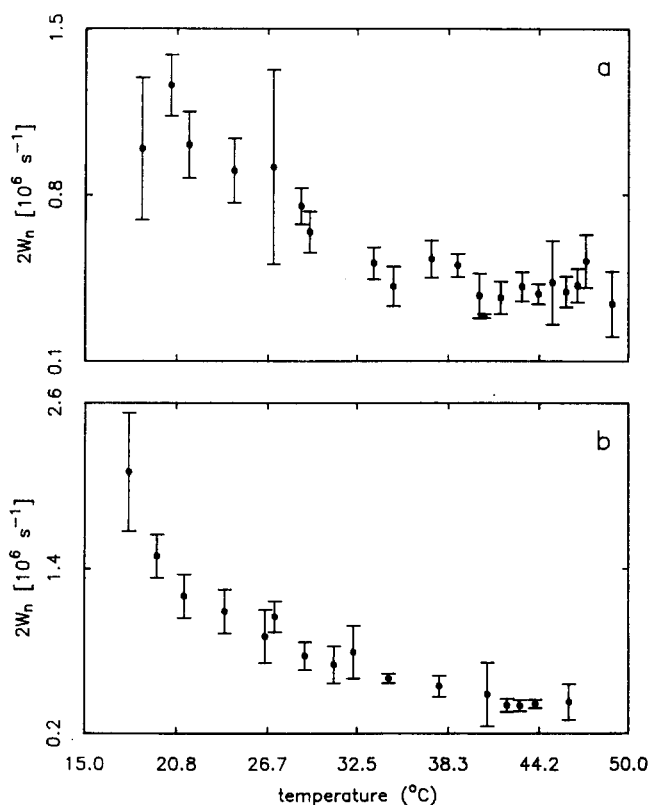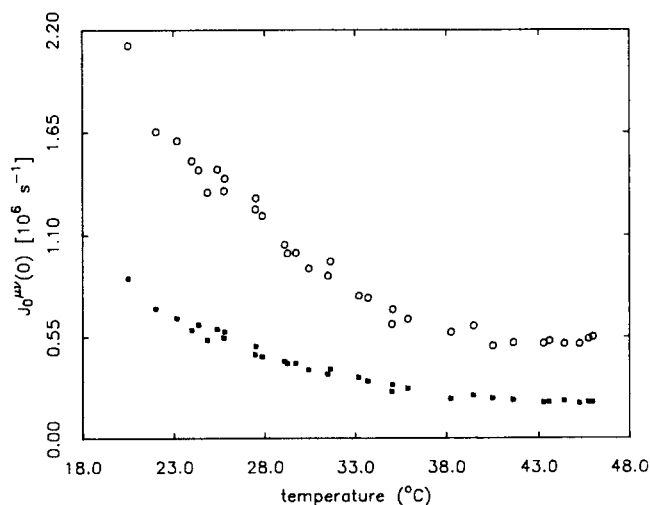

FIG. 8. Zeeman–dipolar spectral densities $-J_0^{DG}(0)$ (solid boxes) and dipolar spectral densities $J_0^{DD}(0)$ (open circles) for PD-tempone in S2.
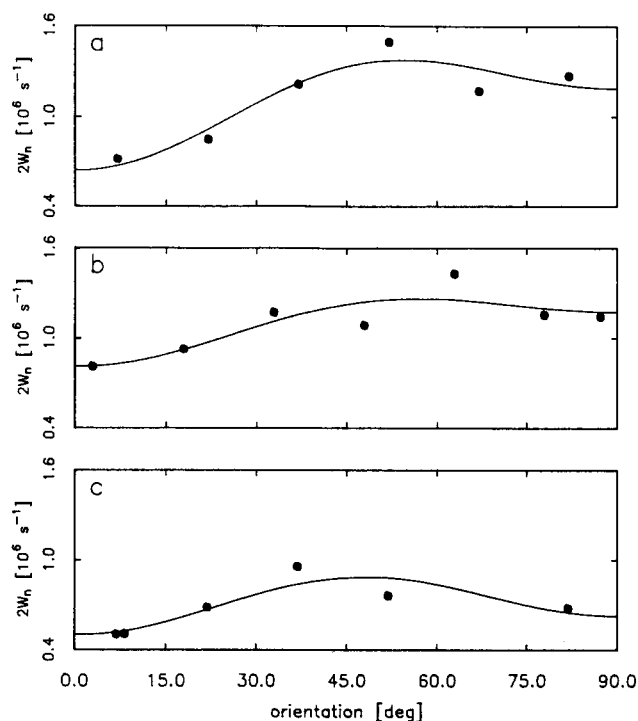
FIG. 9. Orientation dependence of W_n for PD-tempone in S2 at (a) 15.45 ± 0.25; (b) 26.15 ± 0.06; (c) 30.95 ± 0.11 °C.
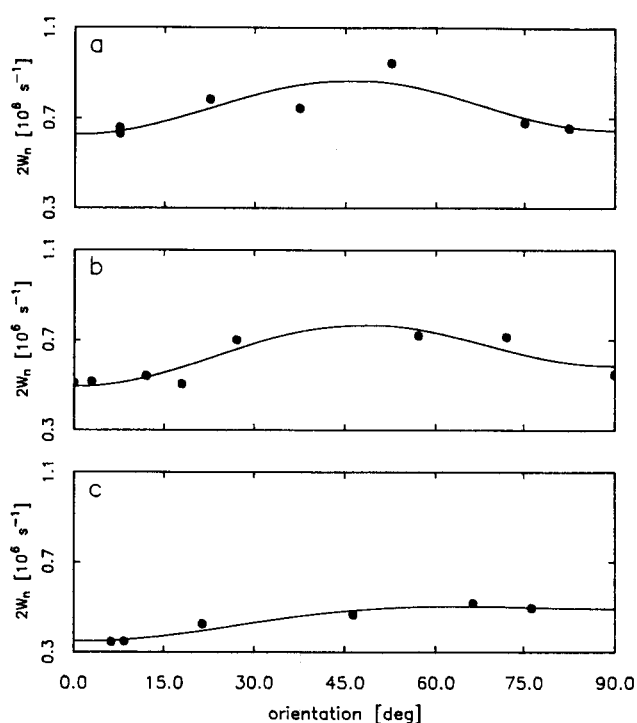

FIG. 10. Orientation dependence of W_n for PD-tempone in S2 at (a) 34.30 ± 0.13; (b) 37.86 ± 0.26; (c) 42.60 ± 0.07 °C.

C. Orientation-dependent relaxation

Orientation–dependent ^{14}N spin–relaxation rates measured at seven temperatures between 15 and 45 °C are illustrated in Figs. 9 and 10 (20.25 ± 0.08 °C not shown). Superimposed on these data are the curves obtained from Eq. (29) with nonlinear least-squares estimates of the dipolar spectral densities $J_0^{DD}(\omega_a)$, $J_1^{DD}(\omega_a)$, and $J_2^{DD}(\omega_a)$ (cf. Table I). These spectral densities are the fundamental spectral densities associated with electron–nuclear dipolar relaxation, since they arise from the END part of the time-dependent spin–Hamiltonian [cf. Eq. (6)]. Figure 11 illustrates the temperature dependence of the dipolar spectral densities. $J_1^{DD}(\omega_a)$ appears to be small throughout the smectic A phase (cf. Table I), indicative of the fact that ODF are suppressed at this frequency, and thus is consistent with the conclusions of Mugele et al.[12]

The qualitative trend of the orientation dependence of W_n (cf. Fig. 9) is not consistent with anisotropic rotational diffusion of the solute. A typical result obtained with that model is illustrated in Fig. 12. The predicted orientation de-

pendence of W_n in the anisotropic diffusion model does depend on details of the intermolecular potential, e.g., on the orientational order parameter S and any asymmetry; however no choice of ordering succeeds in fitting the actual data (even for values not consistent with the observed hyperfine splitting). In attempting to fit the orientation dependent data to a SRLS model, we utilized Eq. (45) and the perturbational expressions of Polnaszek and Freed[56,74] for the $\kappa(K,M)$ in terms of the order parameters[75] $\langle D_{00}^2 \rangle$ and $\langle D_{00}^4 \rangle$. We could not obtain the observed ratios of M-dependent dipolar spectral densities with a SRLS model utilizing Eq. (45), irrespective of the mean-square local order parameter. We have not investigated the effects of incorporating an M dependence of the τ_x in Eqs. (44) and (45),[2] thus we cannot exclude a SRLS mechanism in general. The anisotropic viscosity model was successful in predicting the general appearance of the orientation dependence of W_n, however the magnitude of the orientation dependence was several orders of magnitude too small, i.e., the observed ratios $J_0^{DD}(\omega_a)/J_1^{DD}(\omega_a)$ and $J_2^{DD}(\omega_a)/J_1^{DD}(\omega_a)$ were close to unity. This result was obtained only when $\hat{\tau}_R$ (obtained

TABLE I. Dipolar spectral densities of 2.0×10^{-3} M PD-tempone in S2.

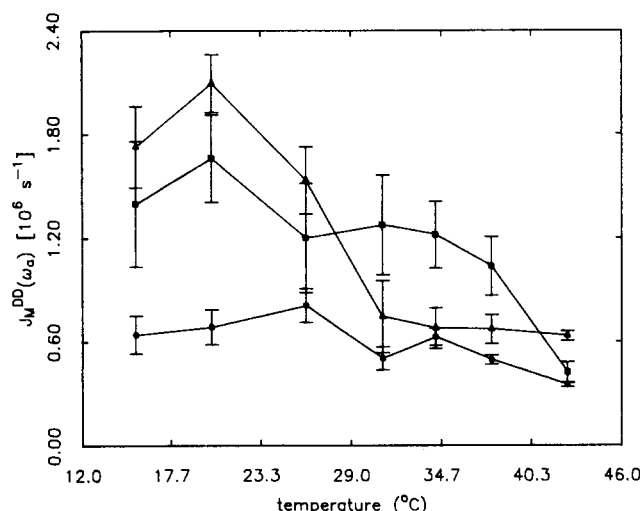| T [°C]	$J_0^{DD}(\omega_A)$ [10^{-6} s^{-1}]	$J_1^{DD}(\omega_a)$ [10^6 s^{-1}]	$J_2^{DD}(\omega_a)$ [10^6 s^{-1}]
15.45 ± 0.25	1.397 ± 0.363	0.641 ± 0.112	1.727 ± 0.237
20.25 ± 0.08	1.658 ± 0.254	0.685 ± 0.103	2.093 ± 0.169
26.15 ± 0.06	1.199 ± 0.316	0.810 ± 0.100	1.531 ± 0.195
30.95 ± 0.11	1.274 ± 0.288	0.503 ± 0.068	0.744 ± 0.210
34.30 ± 0.13	1.217 ± 0.194	0.627 ± 0.051	0.677 ± 0.119
37.86 ± 0.26	1.036 ± 0.171	0.494 ± 0.029	0.671 ± 0.086
42.60 ± 0.07	0.423 ± 0.060	0.349 ± 0.014	0.633 ± 0.030

FIG. 11. Dipolar spectral densities $J_M^{DD}(\omega_a)$ of PD-tempone in S2: $M = 0$ (boxes); $M = 1$ (circles); $M = 2$ (triangles).
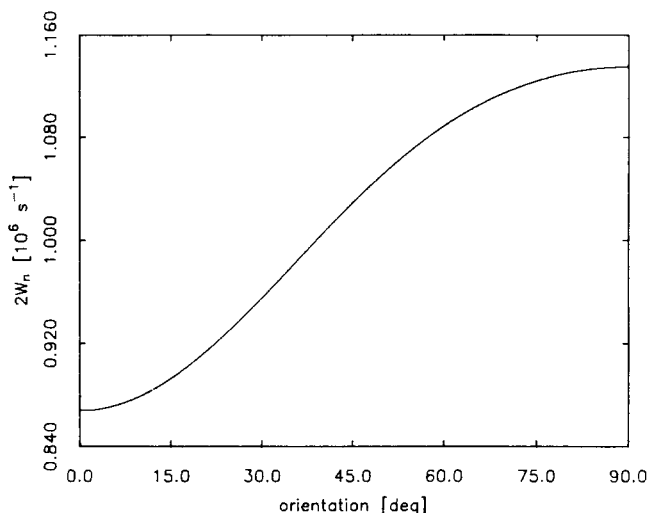

FIG. 12. Simulated orientation dependence of W_n in the anisotropic rotational diffusion model with $\tau_R = 1.29 \times 10^{-10}$ s; $R_\parallel/R_\perp = 0.8$; $S = 0.23$.

from $\widehat{R}$) was roughly the same as τ_R, a regime in which a cross term between anisotropic diffusion and anisotropic viscosity, which was neglected in our calculations, could be important. Thus, we cannot exclude a model of anisotropic viscosity which includes the cross term. However we have no *a priori* reason to believe that such a model would adequately predict our observations. Pretransitional fluctuations[5,23,25] are probably not significant, except perhaps for the 42.6°C data. In any case they should have negligible spectral density at ω_a.[5,23,25]

The model most in agreement with our observed orientation dependence of the W_n is the Moro and Nordio model of rototranslational diffusion. The parameters A, B, and C of the potential given by Eq. (48) were chosen to fit the observed M-dependent spectral densities, and to be consistent with preferential location of the probe molecule in the aliphatic region of the bilayers. We imposed as additional constraints that (1) the translational order parameter γ is constant with temperature; (2) the maximum local orientational order parameter (call it S_{MAX}) is equal to the order parameter for cholestane (call it S_{CSL}) obtained from the orientation dependent hf splittings; and (3) the rotational diffusion anisotropy (i.e., $D_\parallel^R/D_\perp^R$) is temperature independent. The approximation that γ is constant with temperature is likely to be incorrect in the region close to the NA transition, but otherwise seems to be reasonably consistent with McMillan's mean-field expressions deep in the smectic.[45] The second constraint is based on our assumption that the CSL ordering is dominated by coupling to the aromatic core region of the smectic bilayer irrespective of temperature, and that a rather similar potential of mean torque is experienced by PD-tempone *when* it is located in the aromatic core region. The first part of this assumption is reasonable considering that the CSL molecule is comparable in size to the solvent molecules and is highly ordered. The second part may not be entirely satisfactory, considering the different structures of the two probe molecules, but is consistent with our experience with predictions from the Moro–Nordio model. For example, we find that if we use instead the con-

straint that S_{MIN}, occuring at the aliphatic tails, is approximately zero, then the *fits* to the model *predict* an S_{MAX} approximately equal to S_{CSL} (cf. below). The rotational diffusion anisotropy was chosen to be $D_\parallel^R/D_\perp^R = 0.8$ and temperature independent in order to obtain agreement with the observed C/B ratios and our past experience with this spin–probe.[1,4,5,23,66] Once these constraints are imposed, a unique fit to the data may be obtained as follows: (1) choose the sum $A + B$ that predicts S_{MAX} equal to S_{CSL}; (2) choose C such that γ is equal to the desired constant value; (3) choose the difference $A - B$ that predicts the observed ratio $J_2^{DD}(\omega_a)/J_1^{DD}(\omega_a)$; (4) choose τ_R such that $J_1^{DD}(\omega_a)$ is equal to the observed value; and (5) choose D_{zz}^T such that $J_0^{DD}(\omega_a)$ is equal to the observed value and $J_0^{DD}(0)$ is not much larger than $J_0^{DD}(\omega_a)$. This procedure guarantees a unique fit to the data for a *predetermined* γ and $D_\parallel^R/D_\perp^R \equiv N$, i.e., we have the three independent observables $J_0^{DD}(\omega_a)$, $J_1^{DD}(\omega_a)$, and $J_2^{DD}(\omega_a)$, and the three parameters $A - B$, τ_R, and D_{zz}^T. The strategy employed here was to investigate the model's ability to fit the data at all observed temperatures, under the assumption that γ is temperature invariant. Because γ has not been measured, the estimates that we obtain for the varied parameters cannot be taken too seriously, i.e., a completely new set of parameters would be obtained for a different γ. However, we do find that for large γ ($\gamma \approx 0.75$) the predicted $J_0^{DD}(\omega_a)$ is much smaller than the observed value, irrespective of D_{zz}^T. Thus, we have reason to believe that γ should be small (e.g., $\gamma < 0.5$). Also we find for $\gamma \approx 0.75$ that $S_{min} > 0.3$ and that σ is large in magnitude ($\sigma \sim 0.27$ at 15.45 °C) relative to that obtained with $\gamma = 0.294$ ($\sigma = 0.042$ at 15.45 °C). Such a large value of σ, such as that obtained with $\gamma \approx 0.75$, is inconsistent with molecular ordering measurements near the NA transition (cf. Fig. 5) which have shown an absence of enhancement of the orientational order on the smectic A side of the transition. This absence of enhancement in S, due to smaller values of σ, is consistent with the Landau-de Gennes[76] and molecular field[45] theories of the NA transition. It should also be noted

that the value of S required to predict the observed ratio $J_2^{DD}(\omega_a)/J_1^{DD}(\omega_a)$ does not change very much upon increasing γ.

Estimates of the potential parameters A, B, and C, and the diffusion coefficients $D_\parallel^R$, $D_\perp^R$, and D_{zz}^T obtained by simulation are tabulated in Table II along with the order parameters obtained with Eqs. (49)–(51). The precise definitions for these order parameters are:

$$S = Z^{-1} \int_0^d dz \int_0^\pi \sin\beta \, d\beta \, P(\beta, z/d) P_2(\cos\beta), \qquad (56)$$

$$\sigma = Z^{-1} \int_0^d dz \int_0^\pi \sin\beta \, d\beta \, P(\beta, z/d) P_2(\cos\beta) \cos\left(\frac{2\pi z}{d}\right), \qquad (57)$$

$$\gamma = -Z^{-1} \int_0^d dz \int_0^\pi \sin\beta \, d\beta \, P(\beta, z/d) \cos\left(\frac{2\pi z}{d}\right), \qquad (58)$$

with

$$Z = \int_0^d dz \int_0^\pi \sin\beta \, d\beta \, P(\beta, z/d). \qquad (59)$$

These expressions were evaluated numerically using Simpson's rule. [The 34.30 °C data could not be fit under the constraints outlined above because of the anomalously small ratio $J_2^{DD}(\omega_a)/J_1^{DD}(\omega_a)$ obtained at this temperature. The D_{zz}^T required to properly estimate $J_0^{DD}(\omega_a)$ at 42.6 °C is anomalously large, and hence the 42.60 °C results should not be taken seriously. The estimated order parameters and the τ_R at 42.60 °C do, however, seem reasonable in comparison with the other temperatures.]

At the lower temperatures the order parameter S in Table II is larger than that obtained from the hf splittings, but as the temperature increases the two quantities approach one another. We demonstrate this behavior in Fig. 13 where the two estimates of the orientational order parameter are plotted along with the orientational–translational order parameter σ. Also apparent in Fig. 13 is the opposite temperature behavior of S vs σ obtained from the Moro and Nordio model. Similar to the behavior of the two estimates of orientational order parameter illustrated in Fig. 13, S and σ appear to merge as the temperature increases. (Such a temperature dependence of σ is inconsistent with mean-field theory, but it appears consistent with the model of probe expulsion toward the aliphatic chains as T is lowered.)

At first glance at Table II it would appear that the predicted translational diffusion coefficients are in reasonable agreement with what is measured by NMR pulsed field gra-
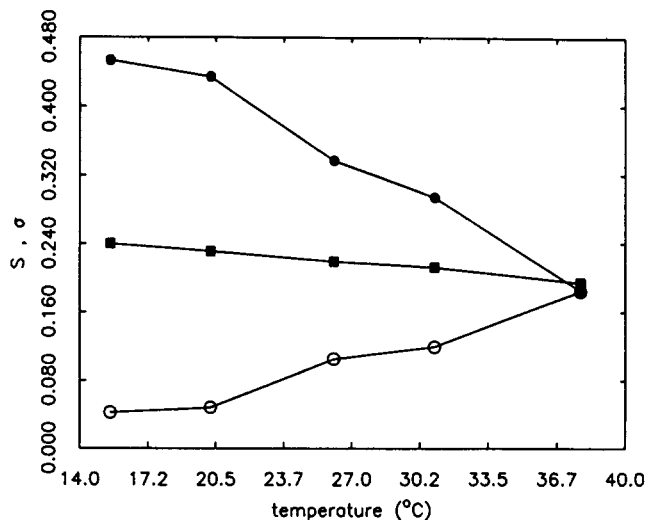

FIG. 13. Orientational order parameters obtained from hf splittings (solid boxes) and from the Moro–Nordio model (solid circles), and the orientational–translational order parameter σ (open circles).

dients[77] and ESR imaging[78] on related mesophases. Closer examination of the theory reveals, however, that we should not make judgments, based on D_{zz}^T, of the agreement between our simulations and the field gradient experiments. What the field gradient experiments measure is the actual transport coefficient $D_\parallel$, whereas what we obtain from Eq. (46) is a microscopic quantity, associated with the time scale over which the probe moves across the spatially nonuniform bilayer. Moro and Nordio[7] obtain the following expression relating D_{zz}^T to $D_\parallel$ in the case of a spherical probe:

$$D_{zz}^T = D_\parallel \int_0^d dz [P^T(z)]^{-1}, \qquad (60)$$

where $P^T(z)$ is defined by

$$P^T(z) = Z^{-1} \int_0^\pi \sin\beta \, d\beta \exp[-U(\beta, z/d)/kT]. \qquad (61)$$

In the nematic phase $P^T(z)$ should be independent of z and $D_{zz}^T = D_\parallel$. In the smectic, however, translation along z is progressively more hindered as $P^T(z)$ becomes more sharply peaked and hence $D_\parallel/D_{zz}^T < 1$. The $P^T(z)$ obtained at 15.45 °C is illustrated in Fig. 14. This reduced distribution function shows the preference of the probe molecule to be located in the hydrocarbon chain region, consistent with the tendency of PD-tempone to be expelled from the aromatic

TABLE II. Parameters obtained from orientation-dependent W_n simulations with the Moro and Nordio model of solute dynamics in smectics.

T [°C]	A	B	C	τ_R [ps]	D_{zz}^T [cm^2 s^{-1}][a]	S	S_{MAX}	σ	γ
15.45	−3.40	−2.73	2.205	131.5	1.14×10^{-6}	0.453	0.823	0.042	0.294
20.25	−3.20	−2.60	2.073	143.4	1.41×10^{-6}	0.434	0.812	0.048	0.294
26.15	−2.60	−2.55	1.820	130.4	3.42×10^{-6}	0.337	0.785	0.105	0.294
30.95	−2.27	−2.40	1.630	76.0	3.08×10^{-6}	0.294	0.759	0.119	0.294
37.86	−1.70	−2.57	1.426	67.8	5.47×10^{-6}	0.185	0.732	0.184	0.294
42.60	−1.52	−2.39	1.299	59.2	$>25\times10^{-6}$	0.167	0.704	0.177	0.294

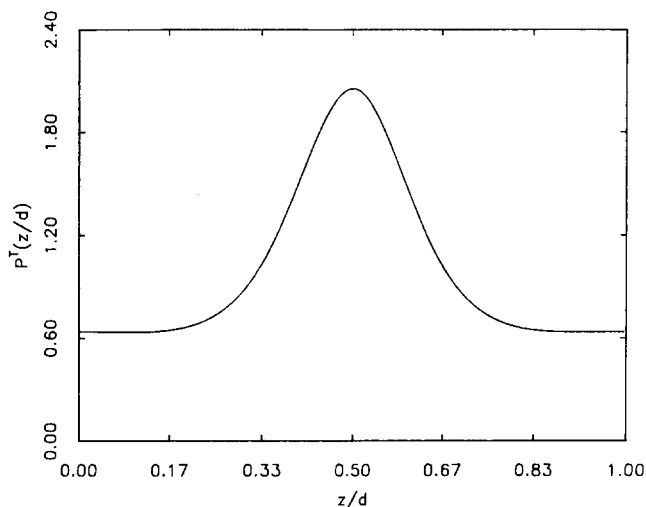[a] Obtained with a bilayer thickness $d = 3.0\times10^{-7}$ cm.

FIG. 14. The reduced distribution function $P^T(z)$ obtained from the Moro–Nordio potential with $A = -3.4$, $B = -2.73$, and $C = +2.205$.
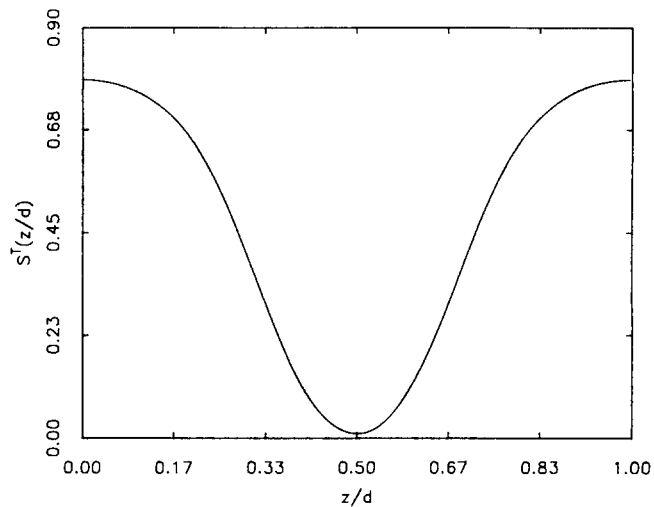

FIG. 15. Spatial variation of the orientational order parameter predicted by the Moro and Nordio model.

core. The $D_\parallel$ computed from the D_{zz}^T according to Eq. (60) are reduced by about 15% in comparison with the D_{zz}^T, falling in the range 0.97×10^{-6} cm^2 s^{-1} $- 4.57 \times 10^{-6}$ cm^2 s^{-1}. These are reasonable values for diffusion coefficients but are somewhat greater than the NMR results of Krüger for parallel diffusion of, e.g., trichlorotrifluoro ethane in the smectic phase of C_{12}-BAA.[77] We obtain for $D_\parallel$ an Arrhenius activation energy $E_a = 12.61 \pm 2.16$ kcal mol^{-1} with a preexponential factor $A = 2981$ cm^2 s^{-1} and for τ_R, $E_a = 6.29 \pm 1.95$ kcal mol^{-1} with $A = 2.83 \times 10^{-15}$ s. The results of Krüger did demonstrate that the self-diffusion coefficients in the smectic phase vary greatly from one mesogen to another. Since Krüger did not present data on PD-tempone in S2 or even a closely related mesogen, we cannot utilize his results to determine the accuracy of our predictions. In any case a more directly relevant experiment is translational diffusion by ESR imaging[78] in which we would obtain $D_\parallel$ for PD-tempone in S2. The results of such an experiment would help to provide a better test of the Moro–Nordio model. A recent result on PD-tempone at 20 °C in the nematic phase of MBBA is of the order of the present estimate of $D_\parallel$ in S2, but roughly half as large.

From the coefficients of the potential given in Table II we obtain the spatial variation of the local orientational order parameter with the expression

$$S^T(z) = \langle \mathscr{D}_{00}^2 (\beta) \rangle_\Omega (z)$$

$$= \frac{1}{P^T(z)} \int_0^\pi \sin \beta \, d\beta$$

$$\times \exp[- U(\beta, z/d)/kT] \mathscr{D}_{00}^2 (\beta), \qquad (62)$$

where $\langle \rangle_\Omega$ denotes an average over the equilibrium distribution of orientations. Figure 15 illustrates the spatial variation of $\langle \mathscr{D}_{00}^2 (\beta) \rangle_\Omega$ for the 26.15 °C data. Note the near absence of orientational order for the probe located in the hydrocarbon region of the bilayer (as mentioned above). We observe the same phenomenon throughout the smectic A phase. The general appearance of Fig. 15 is similar to that obtained by ^{2}H NMR measurements of the segmental order parameter

S_{CD} as a function of deuteron location along the hydrocarbon chain of alkyloxy-cyanobiphenyls (NOCBs)[79] and alkyl-cyanobiphenyls (NCBs).[80]

We can hope to gain additional insight into the solute dynamics by studying the orientation dependence of the zero frequency spectral densities obtained from the linewidth parameters B. The orientation dependences of B and C at 31.3 and 38.5 °C are given in Figs. 16 and 17. At both temperatures there appears to be little orientation dependence of B and C. Nevertheless we proceed to fit the orientation dependent B's to the model independent expression for the angular dependence of $J_0(\omega, \theta)$ [cf. Eq. (30)]. This procedure yields the Zeeman–dipolar spectral densities J_0^{DG}, $J_1^{DG}(0)$, and $J_2^{DG}(0)$ tabulated in Table III. The observed trend $-J_0^{DG}(0) > -J_1^{DG}(0) < -J_2^{DG}(0)$ is predicted by the rototranslational diffusion model with the parameters of Table II; however the magnitudes of the $J_M^{DG}(0)$'s obtained from the rototranslational diffusion model are less than the ex-
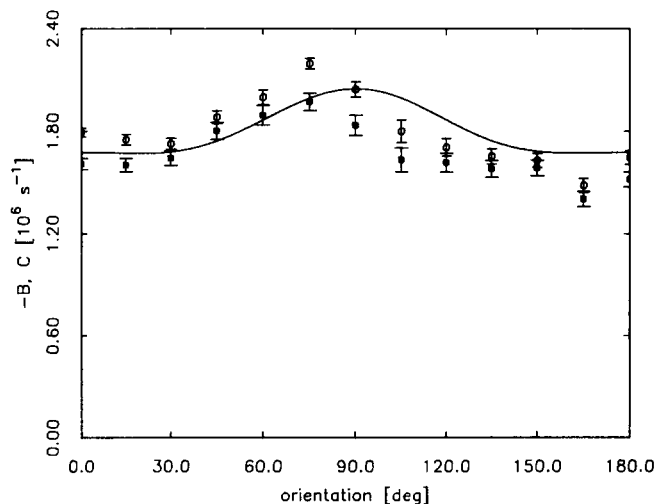

FIG. 16. Orientation dependence of $-B$ (open circles) and C (solid boxes) for PD-tempone in S2 at 31.34 ± 0.05 °C.
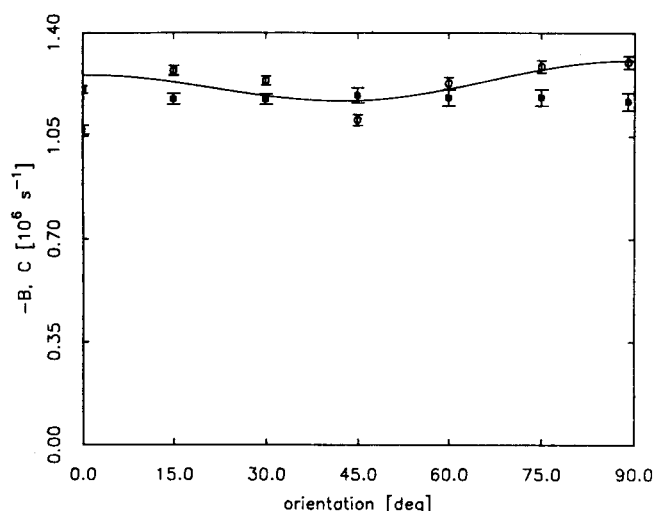
FIG. 17. Orientation dependence of $-B$ (open circles) and C (solid boxes) for PD-tempone in S2 at 38.50 ± 0.20 °C.

perimental values. In addition, the degree of orientation dependence, which is reflected in the ratio of J_2 to J_1, is substantially different at the frequencies zero and ω_a. Also listed in Table III are the dipolar spectral densities $J_M^{DD}(0)$ obtained from the orientation dependent C's and W_n's via Eq. (55). These spectral densities were obtained upon evaluating the model independent expression for $J_1^{DD}(\omega_a,\theta)$ [cf. Eq. (31)] at seven orientations between 0° and 90° utilizing the least-squares estimates of the $J_M^{DD}(\omega_a)$ tabulated in Table I. They do not appear consistent with the trend $J_0 > J_1 < J_2$ observed with the $J_M^{DD}(\omega_a)$ and the $J_M^{DD}(0)$. We cannot be certain if this behavior is due to artifacts or is a manifestation of some K dependence of the spectral densities [cf. Eq. (10)] different from what has been incorporated into our analysis based on the Moro–Nordio model (e.g., due to a lack of axial symmetry of the probe). The rototranslational diffusion model fit with the parameters of Table II predicts a virtually identical magnitude and M dependence of the $J_M^{DD}(\omega)$ over the frequency range $\omega = 0$ to ω_a. Thus the agreement of this model with the experimental $J_M^{DD}(0)$ is less than satisfactory.

The very weak angular dependence of the T_2's (and hence the linewidth parameters) is an especially surprising result considering that: (1) inhomogeneous linewidths obtained from the FIDs for the same sample are orientation dependent; and (2) most models (rotational diffusion as

well as the rototranslational diffusion model) predict substantial angular variation for PD-tempone.[2,7] Lin and Freed[2] do predict an orientation dependent T_2^* (i.e., inverse linewidth including inhomogeneous contributions) upon simulating the effects of a static distribution of director orientations with a magnetic field pulling effect and with an underlying orientation independent T_2. If there is, in fact, a static distribution of directions, we should expect the apparent "homogeneous" linewidths obtained by the CW methods described in Sec. III C to differ from those obtained directly by spin–echoes. In Fig. 18 we illustrate the results of both experiments as a function of temperature. We see in Figs. 18(a) and 18(b) that $T_2(+ 1)$ and $T_2(0)$ obtained by CW methods in the ordered phases are consistently smaller than those obtained by ESE, whereas in the isotropic phase the two methods are in better agreement. The discrepancy in $T_2(0)$ indicates that $A(\mathrm{CW}) > A(\mathrm{ESE})$, and is presumably due to a nuclear spin independent inhomogeneous broadening contribution to $A'(\mathrm{CW})$. This additional broadening does not manifest itself significantly for the $M_I = -1$ hf line [cf. Fig. 18(c)], presumably because the homogeneous width of this hf line is about twice that of the other two lines, and is therefore not as susceptible to distortion by small inhomogeneities. The additional broadening in the CW line shapes is the anticipated result of a static distribution of directors. The CW homogeneous linewidth estimation procedure (cf. Sec. III C and Ref. 2) does not account for any sources of inhomogeneous broadening other than shf structure, and hence incorrectly attributes the broadening resulting from a static distribution of directors to a homogeneous broadening. The most dramatic lack of agreement between CW and ESE measurements is at the low field $(M_I = + 1)$ line. The differing extent of agreement of CW and ESE results at the low field $(M_I = + 1)$ line vs the high field $(M_I = - 1)$ line is suggestive of the C/B anomaly observed in nematics in the incipient slow-tumbling regime,[1] wherein the low field CW ESR line shape deviated dramatically from the theoretical prediction based on isotropic Brownian diffusion in an orienting potential. The connection, if there exists one, between this observation with S2 and those of Polnaszek and Freed with phase V and Lin and Freed[2] in other smectics underscores the importance of further investigation of these materials with the electron spin echo technique.

Although the rototranslational diffusion model can predict the observed $J_M^{DD}(0)$ or the observed $J_M^{DD}(\omega_a)$, it appears that it cannot simultaneously predict $J_M^{DD}(0)$, $J_M^{DG}(0)$

TABLE III. Dipolar and Zeeman–dipolar spectral densities of PD-tempone in S2 obtained from T_2 and W_n results.

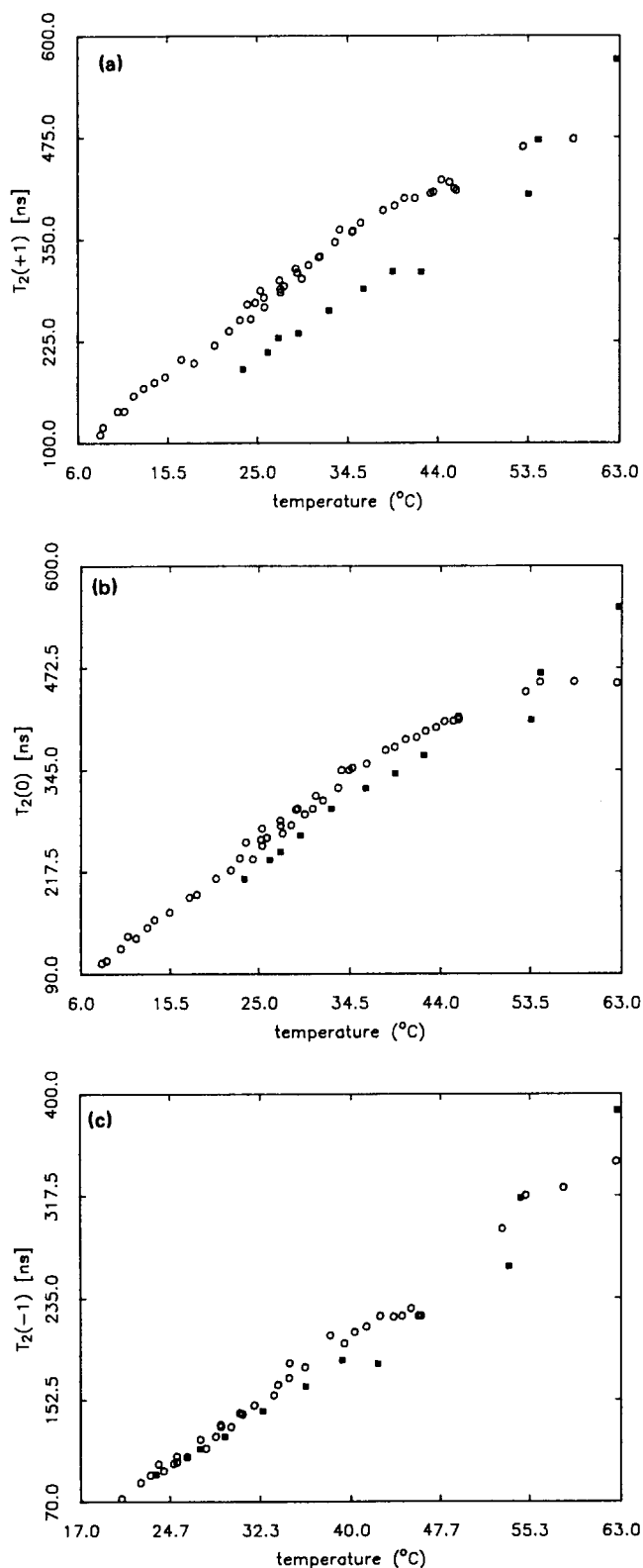| T [°C]	$-J_0^{DG}(0)$ $[10^6 \mathrm{s}^{-1}]$	$-J_1^{DG}(0)$ $[10^6 \mathrm{s}^{-1}]$	$-J_2^{DG}(0)$ $[10^6 \mathrm{s}^{-1}]$
31.34 ± 0.05	0.314 ± 0.015	0.308 ± 0.020	0.407 ± 0.023
38.50 ± 0.25	0.236 ± 0.008	0.211 ± 0.010	0.248 ± 0.010
T [°C]	$J_0^{DD}(0)$ $[10^6 \mathrm{s}^{-1}]$	$J_1^{DD}(0)$ $[10^6 \mathrm{s}^{-1}]$	$J_2^{DD}(0)$ $[10^6 \mathrm{s}^{-1}]$
31.34 ± 0.05	0.778 ± 0.018	1.023 ± 0.023	1.007 ± 0.024
38.50 ± 0.25	0.599 ± 0.092	0.766 ± 0.012	0.669 ± 0.012

FIG. 18. T_2's estimated from CW ESR (solid boxes) and measured by ESE methods (open circles) for PD-tempone in S2: (a) $M_I = +1$; (b) $M_I = 0$; (c) $M_I = -1$.

densities at zero frequency appear for the most part to be larger than those at ω_a. This is suggestive of a second dynamical mechanism which selectively enhances the spectral densities at zero frequency [the rototranslational diffusion simulations give $j_M(0) \simeq j_M(\omega_a)$]. Such a mechanism would have to be relatively slow in order to affect predominantly $j_M(0)$, and might be associated with a SRLS effect due to fluctuations of the aliphatic chain. Given the poor probe ordering in the hydrocarbon chains (predicted by the rototranslational diffusion model), we expect to observe an orientation dependence of the $j_M(0)$ which is weaker than that anticipated from the order parameter S obtained from hf splittings. These properties motivate a closer examination of the hydrocarbon SRLS mechanism.

The SRLS effect associated with slow collective motions of the hydrocarbon chains, which persist for a mean time τ_x, could enhance the relaxation dispersion at zero frequency, thereby contributing to the $j_M(0)$ while having a lesser effect on the $j_M(\omega_a)$ (i.e., $\omega_a^2 \tau_x^2 > 1$). In addition, the SRLS modes should suppress the orientational order parameter that is obtained from the hf splittings in an analogous fashion to ODF [cf. Eq. (40)]. In other words, the measurable order parameter $\tilde{S}$ is less than S. Let us assume for simplicity (see below) that the Plomp and Bulthuis expression for $\tilde{S}$ in terms of S [cf. Eq. (40)] may be adapted for SRLS by replacing $\langle|\Theta|^2\rangle$ with $\langle|S_l|^2\rangle$. Then we obtain the expression

$$\langle|S_l|^2\rangle \approx \tfrac{2}{3}(1 - \tilde{S}/S) \tag{63}$$

relating the mean-squared amplitude of the local structure fluctuations to the order parameters $\tilde{S}$ and S obtained from hf splittings and Moro–Nordio model simulations, respectively. Figure 19 illustrates the behavior predicted by Eq. (63) of the mean-squared local structure fluctuations with temperature. We see that the local structure fluctuations decay with increasing temperature until reaching zero mean squared amplitude at about 38.5 °C [cf. Fig. 8 vs Fig. 6(a)]. This behavior is roughly consistent with the observation that the ratio $J_0^{DD}(0)/J_1^{DD}(\omega_a)$ decreases from a value of about two at 20 °C to about one at 38.5 °C, due presumably to a
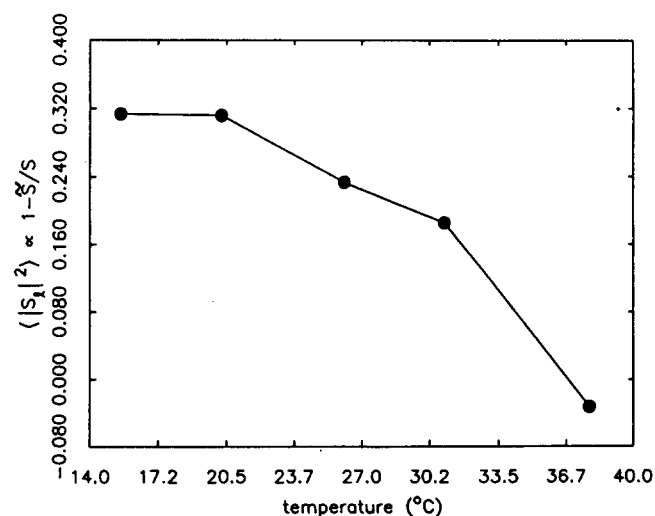

FIG. 19. Approximate mean-squared amplitude of SRLS fluctuations in S2.

and $J_M^{DD}(\omega_a)$ with a unique set of parameters. The distinctions between $J_M^{DD}(0)$ and $J_M^{DD}(\omega_a)$ are twofold, first, as stated above the magnitude of the orientation dependence at zero frequency is less than at ω_a; and second, the spectral

deterioration of the SRLS modes, which enhance predominantly $j(0)$. It does not explain, however, the observation that at 38.5 °C there is very little orientation dependence of the linewidth parameters. At this temperature $\langle |S_l|^2 \rangle \sim 0$ and the B parameter is predicted by the rototranslational diffusion model to have some orientation dependence. This is not borne out in our 38.5 °C data. This discrepancy between model and experiment warrants further investigation. However until we obtain further experimental data of a different nature (e.g., diffusion coefficients by ESR imaging and x-ray determination of smectic order parameters of the solvent) an explanation of this observation would be too speculative. In consideration of the other data, we suggest a model in which the T_2's are affected by a slowly relaxing local hydrocarbon structure, which has appreciable local order that is averaged out over a longer time scale, and the W_n's are dominated by the rototranslational diffusion of the probe molecule in the spatially nonuniform smectic.

In order to describe such a composite process involving both rototranslational diffusion and cooperative hydrocarbon chain fluctuations, we must recognize an important ingredient that is not correctly accounted for in our analysis. A correct description would require the incorporation of cooperative hydrocarbon chain distortions,[28] wherein the hydrocarbon chains are *tilted* with respect to the z direction by Ω', with some short range but no long range order in Ω'. Translational diffusion of the probe perpendicular to the z direction will lead to a SRLS mechanism, wherein the tilt Ω' of the local ordering changes with time as the probe moves through the bilayer. Furthermore, an isotropic averaging over all orientations Ω' of tilt, would be the appropriate sources of the renormalized order parameter such as is expressed by Eq. (63). In the Moro–Nordio model, no such tilt was introduced, for simplicity. (Another generalization of the Moro and Nordio expressions of some physical importance would be to account for the spatial variation of microscopic viscosity parallel to the z direction with the incorporation of a z-dependent τ_R.)

Although we do not claim to have exhausted all plausible models of the microscopic dynamics (indeed we have not), we do believe that the Moro–Nordio model provides a satisfactory physical picture of solute diffusion in the smectic A phase. It accounts for translational diffusion of the spin–probe perpendicular to the plane of the layers, and for the lack of spatial uniformity of the torques experienced by the probe as it translates. It accounts for the positional ordering of the solvent molecules in the smectic phases. It predicts the expulsion of the spin–probe molecule from the aromatic core region of the bilayers, as suggested by several investigators.[2,30] It does not account, however, for the observed weak orientation dependence of the T_2's.

We have a few additional comments. First of all, throughout the analysis of 2D ELDOR spectra we have neglected nuclear spin dependent nonsecular terms arising from motional averaging of the electron–nuclear dipolar interaction (cf. Sec. IV A). However, there is no evidence in the 2D ELDOR data that such terms are significant. [Nuclear spin dependent nonsecular terms are predicted by theory to influence the pattern of 2D ELDOR cross peaks (cf.

Appendix A).] Furthermore, given the results of the rototranslational diffusion simulations, we find an *a posteriori* self-consistency in that such terms, which depend solely on the spectral densities at the ESR frequency ω_e, are reduced by a factor of 20–30 with respect to the spectral densities at ω_a. Thus they should be too small to detect within our present experimental uncertainty.

Finally, we recall that throughout the analysis we have neglected the effects of nuclear spin quantization on the theoretical treatment of the angular dependences.[54] One would conclude from the weak orientational ordering deduced from the hf splittings (cf. Fig. 5) that neglect of such effects is fully justified. However, if one considers the spatial variation of S predicted by the rototranslational diffusion model, then the effects of ^{14}N spin–quantization might be significant when the probe experiences the strong local ordering near the solvent aromatic core. In the present work we note that the probe is found to have a low probability of location near the aromatic core, and that when averaged over the bilayer the orientational order parameters obtained from simulation are still not very great, especially at high temperature. The motional narrowing theory therefore seems adequate for the interpretation of our data. A complete theoretical treatment of the problem would, however, have to properly account for the full effects of spin quantization.

V. SUMMARY

Utilizing electron spin–echo and two-dimensional Fourier transform ESR techniques we have obtained homogeneous linewidths and ^{14}N spin–relaxation rates for the radical PD-tempone as a function of temperature and director orientation in the smectic phase of S2. We find that the estimated homogeneous linewidths obtained by CW ESR methods are systematically larger than those obtained directly by ESE in the ordered phases, whereas in the isotropic phase the two methods are in better agreement. We attribute these observations to a static distribution of director orientations associated with a distribution of uniformly oriented domains which broadens the CW ESR linewidths. We observe a strong orientation dependence of the W_n's throughout the smectic A phase, whereas the T_2 parameters are only weakly orientation dependent. We find that a model of rototranslational diffusion in a McMillan-type potential accurately predicts the observed magnitude and orientation dependence of the W_n's, which however is not consistent with the homogeneous T_2 parameters. We attribute some of the inconsistency to an additional dynamical process described by a slowly relaxing local structure model of cooperative hydrocarbon chain motion and reorientation. The composite process can be described as one in which the linewidths are influenced by rotational diffusion of the probe modulated by a slowly relaxing local hydrocarbon structure, which has appreciable local order but when averaged over the sample is isotropic, whereas the W_n's are dominated by rototranslational diffusion of the probe molecule in the spatially nonuniform smectic.

ACKNOWLEDGMENTS

APPENDIX A: THE ANALYSIS OF 2D ELDOR

For a nitroxide with three well-separated hf lines the time evolution of the instantaneous electron spin state populations is governed by[34,69]

$$\frac{d}{dt}\tilde{\chi}(t) = -\mathbf{W}\tilde{\chi}(t), \tag{A1}$$

where the matrix $\mathbf{W}$ is the transition probability matrix, whose $\alpha\beta$ th element for $\alpha \neq \beta$ is just minus the transition probability from state β to state α. The vector $\tilde{\chi}(t)$ of populations and the matrix $\mathbf{W}$ are defined in the "eigenstate space" of dimension $A = (2I+1)\times(2S+1)$.[34]

Let us partition $\mathbf{W}$ according to $M_s = \pm 1/2$, then

$$\begin{pmatrix} \dot{\chi}_+(t) \\ \dot{\chi}_-(t) \end{pmatrix} = -\begin{pmatrix} \mathbf{W}_{+,+} & \mathbf{W}_{+,-} \\ \mathbf{W}_{-,+} & \mathbf{W}_{-,-} \end{pmatrix}\begin{pmatrix} \chi_+(t) \\ \chi_-(t) \end{pmatrix}. \tag{A2}$$

We now define new subvectors $\chi^\pm(t)$ of dimension $A/2$ by

$$\chi^\pm(t) = \frac{1}{\sqrt{2}}(\chi_+ \pm \chi_-), \tag{A3}$$

and transform Eq. (A2) to obtain the matrix $\overline{\mathbf{W}}$ defined in the $\chi^\pm$ basis

$$\overline{\mathbf{W}} = \begin{pmatrix} \tilde{\mathbf{W}} & \mathscr{W}^T \\ \mathscr{W} & \hat{\mathbf{W}} \end{pmatrix}, \tag{A4}$$

where

$$2\tilde{\mathbf{W}} = (\mathbf{W}_{+,+} + \mathbf{W}_{-,-} + \mathbf{W}_{+,-} + \mathbf{W}_{-,+}), \tag{A5}$$

$$2\hat{\mathbf{W}} = (\mathbf{W}_{+,+} + \mathbf{W}_{-,-}) - (\mathbf{W}_{+,-} + \mathbf{W}_{-,+}), \tag{A6}$$

$$2\mathscr{W} = (\mathbf{W}_{+,+} - \mathbf{W}_{-,-}) + (\mathbf{W}_{+,-} - \mathbf{W}_{-,+}). \tag{A7}$$

The solution of Eq. (A2) in this new representation is given by

$$\begin{pmatrix} \chi^+(t) \\ \chi^-(t) \end{pmatrix} = \begin{pmatrix} \chi^+(0) \\ \chi^-(0) \end{pmatrix}\exp\begin{pmatrix} -\tilde{\mathbf{W}}t & -\mathscr{W}^T t \\ -\mathscr{W}t & -\hat{\mathbf{W}}t \end{pmatrix}, \tag{A8}$$

or equivalently (for $A = 6$, i.e., a nitroxide)

$$\chi_i(T) = \sum_{k=1}^{6} [\exp(-\overline{\mathbf{W}}T)]_{ik}\chi_k(0)$$

$$= \sum_{j,k=1}^{6} O_{d,ji}\exp(-T/\tau_j)O_{d,jk}\chi_k(0). \tag{A9}$$

The 3×3 matrix $\mathbf{Q}(T)$ of volume integrals obtained from the 2D ELDOR spectrum is proportional to the matrix partition of $[\exp(-\overline{\mathbf{W}}T)]$ associated with the population differences, i.e.,[41,70]

$$Q_{nm}(T) = \epsilon[\exp(-\overline{\mathbf{W}}T)]_{n+3,m+3}$$

$$= \epsilon\sum_{j=1}^{6} O_{d,j,(m+3)}O_{d,j,(n+3)}\exp(-T/\tau_j), \tag{A10}$$

where ϵ is a spectrometer constant. [The matrix $\mathbf{Q}$ is defined such that Q_{mj} is the volume integral of the cross peak located at coordinates $(\omega_1,\omega_2) = (\omega_j,\omega_m)$.] Hence a full analysis of 2D ELDOR nitroxide spectra in the case of three well-separated hf lines requires that we solve the "inverse transform" of Eq. (A10), i.e., we need the normal modes, given by the vectors $O_{d,j}$ (with components $O_{d,ji}$) and their eigenvalues τ_j in terms of the observables $Q_{nm}(T)$.

1. Negligible nonsecular terms

Let us examine the case in which nuclear spin dependent nonsecular contributions (e.g., electron–nuclear dipolar cross relaxation[34]) may be neglected (as is often the case for nitroxides). Then the submatrix $\mathscr{W}$ in Eq. (A8) vanishes and hence the population differences evolve independently and are governed only by the 3×3 submatrix $\hat{\mathbf{W}}$. This results in a particularly simple form for the matrix of 2D ELDOR volume integrals in that we obtain.

$$\mathbf{Q}(T) = \epsilon[\exp(-\hat{\mathbf{W}}T)]. \tag{A11}$$

In order to evaluate the exponential we utilize the eigenvalue decomposition of $\hat{\mathbf{W}}$ given by

$$O_{d,nm} = \begin{matrix} & 1 & 2 & 3 \\ -1 \\ 0 \\ +1 \end{matrix}\begin{pmatrix} 3^{-1/2} & 2^{-1/2} & 6^{-1/2} \\ 3^{-1/2} & 0 & -2(6)^{-1/2} \\ 3^{-1/2} & -2^{-1/2} & 6^{-1/2} \end{pmatrix} \tag{A12}$$

and

$$\tau_1^{-1} = 2W_e, \tag{A13}$$

$$\tau_2^{-1} = 2W_e + 2W_n + \omega_{\text{HE}}, \tag{A14}$$

$$\tau_3^{-1} = 2W_e + 6W_n + \omega_{\text{HE}} \tag{A15}$$

and we can write analytical expressions to obtain W_n and ω_{HE}. Note that in Eq. (A12) we have relabeled the rows of the relevant part of the partitioned matrix, $\mathbf{O}_d$ according to M_I value. Now let us solve Eq. (A11) for the elements of $\hat{\mathbf{W}}$, which we rewrite as matrix elements:

$$[\exp(-\hat{\mathbf{W}}T)]_{nm} = \epsilon^{-1}Q_{nm}(T). \tag{A16}$$

The matrix elements appear in Table IV. To eliminate the unknown constant ϵ we normalize $\mathbf{Q}(T)$ by forming volume ratios, i.e., we define a normalized matrix of volume integrals $\hat{\mathbf{Q}}(T)$ by

$$\hat{Q}_{nm}(T) = \frac{Q_{nm}(T)}{Q_{22}(T)} = \frac{[\exp(-\hat{\mathbf{W}}T)]_{nm}}{[\exp(-\hat{\mathbf{W}}T)]_{22}}, \tag{A17}$$

or equivalently,

$$[\exp(-\hat{\mathbf{W}}T)]_{nm} = \hat{Q}_{nm}(T)[\exp(-\hat{\mathbf{W}}T)]_{22}. \tag{A18}$$

Thus we generate a set of eight independent equations from which to extract the elements of $\hat{\mathbf{W}}$.

In order to account for off-resonance effects and for the

TABLE IV. Matrix elements: $\epsilon^{-1}Q_{nm}(T)$.[a]

Autopeaks[b]	
$\epsilon^{-1}Q_{\pm 1, \pm 1}$:	$\frac{1}{4}\exp[-T/\tau_1] + \frac{1}{2}\exp[-T/\tau_2] + \frac{1}{6}\exp[-T/\tau_3]$
$\epsilon^{-1}Q_{0,0}$:	$\frac{1}{3}\exp[-T/\tau_1] + \frac{2}{3}\exp[-T/\tau_3]$

Cross peaks	
$\epsilon^{-1}Q_{0, \mp 1} = \epsilon^{-1}Q_{\mp 1,0}$:	$\frac{1}{3}\exp[-T/\tau_1] - \frac{1}{3}\exp[-T/\tau_3]$
$\epsilon^{-1}Q_{\pm 1, \mp 1}$:	$\frac{1}{4}\exp[-T/\tau_1] - \frac{1}{2}\exp[-T/\tau_2] + \frac{1}{6}\exp[-T/\tau_3]$

[a] This is the case of negligible nonsecular terms.
[b] These apply both to 2D ELDOR and to stimulated echoes from the three hyperfine lines (cf. Sec. IV A).

effects of spectrometer dead time we generalize Eq. (A18) to obtain

$$V_n V_m^2 r_{1_m} r_{2_n} [\exp(-\hat{\mathbf{W}}T)]_{nm}$$
$$= \hat{Q}_{nm}(T) V_2^3 r_{1_2} r_{2_2} [\exp(-\hat{\mathbf{W}}T)]_{22}, \qquad (A19)$$

where the V_i account for rotation of the ith hf line by less than $\pi/2$ [41] and where r_{1_i} and r_{2_j} are dead time reduction factors. [In the case of Lorentzian (inhomogeneous) line shapes, such as we observe for PD-tempone in S2, the reduction of observed peak areas due to dead times in t_1 and t_2 time domains are given by

$$r_{1_i} = \exp(-\tau_{d_1}/T_{2_i}^*), \qquad (A20)$$

$$r_{2_j} = \exp(-\tau_{d_2}/T_{2_j}^*), \qquad (A21)$$

where τ_{d_1} and τ_{d_2} are the dead times in t_1 and t_2. Equations (A20) and (A21) follow from the more detailed expressions for 2D ELDOR such as given by Eqs. (26) and (27) in Ref. 41.] When Eq. (A19) is appropriate (i.e., when nuclear spin dependent nonsecular terms are negligible), it is convenient to use the related expression

$$V_n r_{2_n} [\exp(-\hat{\mathbf{W}}T)]_{nm}$$
$$= \frac{Q_{nm}(T)}{Q_{mm}(T)} V_m r_{2_m} [\exp(-\hat{\mathbf{W}}T)]_{mm} \qquad (A22)$$

which linearizes Eq. (A19) with respect to the V_i and eliminates r_1 [cf. Eq. (A20)]. Hence with the utilization of Eq. (A22), no explicit knowledge of the dead times in t_1 and t_2 is required for the analysis, only the products $V_i r_{2_i}$, which are easily measured (see below). To utilize Eq. (A22) we form the volume ratio of the cross-peak at coordinates $(\omega_1, \omega_2) = (\omega_m, \omega_n)$ to the autopeak at (ω_m, ω_m).

In the simple case where W_n is negligible and Heisenberg exchange is the only source of magnetization transfer we utilize Eq. (A19) to obtain

$$\frac{1}{3}V_m r_{2_m} \exp(-2W_e T)[1 - \exp(-\omega_{HE}T)]$$
$$= \frac{1}{3}f_{mj}V_j r_{2_j} \exp(-2W_e T)$$
$$\times [1 + 2\exp(-\omega_{HE}T)], \qquad (A23)$$

where $f_{mj} \equiv Q_{mj}/Q_{jj}$. The W_e factor conveniently drops out (so a knowledge of W_e is not needed nor obtained) after which some algebra leads to the expression

$$\omega_{HE} = \frac{1}{T}\ln\left(\frac{2f_{mj}V_j r_{2_j} + V_m r_{2_m}}{V_m r_{2_m} - f_{mj}V_j r_{2_j}}\right). \qquad (A24)$$

The products $V_i r_{2_i}$ are determined by measuring the normalized peak areas obtained from a single pulse FID collected under the same conditions (i.e., same dead time, pulse length, microwave frequency, cavity tuning, etc.) as the 2D ELDOR spectrum.[84] Since we obtain a direct measurement of the $V_i r_{2_i}$ for each hyperfine line i, there is no requirement that the inhomogeneous line shapes be Lorentzian, or even that the line shapes be of a known functional form, in order to utilize the above expressions for the determination of W_n and ω_{HE}. One can easily show (see Appendix B) that the peak areas necessary for the determination of the $V_i r_{1_i}$, $V_j r_{2_j}$, and the matrix $\hat{Q}(T)$ are invariant to the nature and the extent of inhomogeneous broadening, provided that the hyperfine lines remain well separated.

Notice that Eq. (A24) predicts that all six cross peaks equivalently reflect the exchange process, and hence that six independent measurements of the exchange rate ω_{HE} are obtained from a single 2D spectrum. The equivalence of the six cross peaks is a manifestation of the lack of a selection rule for the exchange mechanism,[81] i.e., both $\Delta M_I = \pm 1$ and $\Delta M_I = \pm 2$ transitions are equally probable. In the more general case of nonnegligible W_n we obtain eight equations analogous to Eq. (A23) which are linear in the two unknowns W_n and ω_{HE}. In this case a linear least-squares procedure may be utilized to determine the minimum two-norm estimates of W_n and ω_{HE}. The W_n mechanism and the exchange mechanism may usually be distinguished in these spectra as a result of their different selection rules. Unlike exchange, the W_n mechanism obeys the selection rule $\Delta M_I = \pm 1$ and thus gives rise predominantly to cross peaks connecting only adjacent hf lines (cf. Fig. 3), but see below. Thus the geometrical pattern of the spectral contours may be utilized to obtain information regarding the mechanism of magnetization transfer prior to the application of Eq. (A23) or its analogues for $W_n \neq 0$. If we consider, for example, a case where only cross peaks for which $\Delta M_I = \pm 1$ are observed, we can utilize Eq. (33) to obtain W_n directly from two of the four cross peaks. The expression for the other two cross peaks (i.e., $m = 0, j = \pm 1$), is somewhat more complicated in that it depends on terms both linear and cubic in $\exp(-W_n T)$, as can be seen by straightforward application of Eq. (A22). These cross peaks nevertheless do directly yield W_n, provided exchange is absent. The full set of linear equations applicable when $\omega_{HE} \neq W_n \neq 0$ and when nuclear spin dependent nonsecular terms may be neglected is then given by

$$(2f_{+1,0} + V_{+1}r_{2_{+1}})c = (V_{+1}r_{2_{+1}} - f_{+1,0}), \tag{A25}$$

$$(2f_{-1,0} + V_{-1}r_{2_{-1}})c = (V_{-1}r_{2_{-1}} - f_{-1,0}), \tag{A26}$$

$$\frac{3}{2}(f_{0,+1}V_{+1}r_{2_{+1}})b + (1 + \tfrac{1}{2}f_{0,+1}V_{+1}r_{2_{+1}})c$$
$$= (1 - f_{0,+1}V_{+1}r_{2_{+1}}), \tag{A27}$$

$$\frac{3}{2}(f_{0,-1}V_{-1}r_{2_{-1}})b + (1 + \tfrac{1}{2}f_{0,-1}V_{-1}r_{2_{-1}})c$$
$$= (1 - f_{0,-1}V_{-1}r_{2_{-1}}), \tag{A28}$$

$$\frac{1}{2}(V_{+1}r_{2_{+1}} + f_{+1,-1}V_{-1}r_{2_{-1}})b$$
$$+ \frac{1}{6}(f_{+1,-1}V_{-1}r_{2_{-1}} - V_{+1}r_{2_{+1}})c$$
$$= \frac{1}{3}(V_{+1}r_{2_{+1}} - f_{+1,-1}V_{-1}r_{2_{-1}}), \tag{A29}$$

$$\frac{1}{2}(V_{-1}r_{2_{-1}} + f_{-1,+1}V_{+1}r_{2_{+1}})b$$
$$+ \frac{1}{6}(f_{-1,+1}V_{+1}r_{2_{+1}} - V_{-1}r_{2_{-1}})c$$
$$= \frac{1}{3}(V_{-1}r_{2_{-1}} - f_{-1,+1}V_{+1}r_{2_{+1}}), \tag{A30}$$

where $b = \exp[-(2W_n + \omega_{HE})T]$ and $c = \exp[-(6W_n + \omega_{HE})T]$. Thus, upon solving the overdetermined system of linear equations we obtain W_n and ω_{HE} from the expressions

$$2W_n = \frac{1}{2T} \ln\left(\frac{b}{c}\right) \tag{A31}$$

and

$$\omega_{HE} = \frac{1}{2T}(\ln c - 3\ln b). \tag{A32}$$

The presence of cross-peak intensity at $\Delta M_I = \pm 2$ does not necessarily imply the presence of Heisenberg exchange; the W_n mechanism may also contribute intensity to these peaks by a small amount, but only for sufficiently long mixing times T, i.e., when $W_n T > 1$, (cf. Table IV) whereas in the present work T was selected to maximize the other peaks, and this led to $W_n T < 1$. The absence of $\Delta M_I = \pm 2$ peaks for $W_n T \ll 1$ is easily shown by expanding $Q_{\pm 1, \mp 1}$ given in Table IV to lowest power in $W_n T$. [As a final note, we first recall that in nitroxides, the effects of the ^{14}N electric quadrupolar interaction are insignificant.[1] However, if they were not, they could be distinguished from the electron–nuclear dipolar contributions to W_n by their different selection rules[82] (i.e., $\Delta M_I = \pm 2$ is allowed) in cases where ω_{HE} is negligible, e.g., low concentrations of spin–probe.]

2. Perturbational treatment of nonsecular terms

When the nuclear spin dependent nonsecular contributions cannot be neglected, the eigenvalue problem of Eq. (A1) should be solved, followed by substitution of the resulting $O_{d,ij}$ and τ_j into Eq. (A10). If these nonsecular terms are small compared to $2W_e$ we may treat them as perturbations. The six unperturbed (zeroth order) eigenvalues are

$$E_1^{(0)} = 0, \tag{A33}$$

$$E_2^{(0)} = 2W_n + \omega_{HE}, \tag{A34}$$

$$E_3^{(0)} = 6W_n + \omega_{HE}, \tag{A35}$$

$$E_4^{(0)} = 2W_e, \tag{A36}$$

$$E_5^{(0)} = 2W_e + 2W_n + \omega_{HE}, \tag{A37}$$

$$E_6^{(0)} = 2W_e + 6W_n + \omega_{HE}, \tag{A38}$$

where $W_e \equiv W_e(M_I = 0)$. $E_1 = 0$ insures conservation of probability.

The zeroth order eigenvectors are defined by

$$(\psi_1^{(0)},...,\psi_6^{(0)}) \equiv \begin{pmatrix} O_d & 0 \\ 0 & O_d \end{pmatrix}, \tag{A39}$$

where the 3×3 matrix partition O_d is defined in Eq. (A12). Using standard methods[83] we find the first order corrections to the eigenvalues

$$E_1^{(1)} = 0, \tag{A40}$$

$$E_2^{(1)} = W_x^+/2, \tag{A41}$$

$$E_3^{(1)} = 3W_x^+/2, \tag{A42}$$

$$E_4^{(1)} = 4W_x^+/3 + 2W_e\delta^+/3, \tag{A43}$$

$$E_5^{(1)} = W_x^+/2 + W_e\delta^+, \tag{A44}$$

$$E_6^{(1)} = W_x^+/6 + W_e\delta^+/3, \tag{A45}$$

where $W_x^+ \equiv (W_{x_1} + W_{x_2})$ and $\delta^+ \equiv [\delta(+1) + \delta(-1)]$. W_{x_1} and W_{x_2} are the cross-relaxation rates associated with $I_{\mp}S_{\pm}$ and $I_{\pm}S_{\pm}$, respectively, whereas $\delta(+1)$ and $\delta(-1)$ (where $\delta(M_I) = [W_e(M_I) - W_e(0)]/W_e(0)$) are the corrections to W_e at the $M_I = \pm 1$ hf lines arising from electron–nuclear dipolar (END) terms and Zeeman–dipolar cross terms in the spin Hamiltonian.[34] We see from Eqs. (A40)–(A45) that the conditions $W_x^+/W_e \ll 1$ and $\delta^+ \ll 1$ are necessary for perturbation theory to apply. Because of the additional nuclear spin independent contribution to W_e arising from the spin-rotation mechanism[34,52] (call it W_e^{SR}), this first-order treatment is expected to be fairly accurate for nitroxides for which W_e^{SR} is substantial. Note that the first order effects of the perturbation on the eigenvalues depend only on the mean of W_{x_1} and W_{x_2} and of $\delta(+1)$ and $\delta(-1)$ (and not their differences).

The first order corrections to the eigenvectors are

$$\psi_1^{(1)} = 0, \tag{A46}$$

$$\psi_2^{(1)} = \frac{2}{\sqrt{6}}\left(\frac{W_x^-}{E_2^{(0)} - E_4^{(0)}}\right)\psi_4^{(0)}$$
$$- \frac{\sqrt{3}}{6}\left(\frac{W_x^-}{E_2^{(0)} - E_6^{(0)}}\right)\psi_6^{(0)}, \tag{A47}$$

$$\psi_3^{(1)} = \frac{\sqrt{3}}{2}\left(\frac{W_x^-}{E_3^{(0)} - E_5^{(0)}}\right)\psi_5^{(0)}, \tag{A48}$$

$$\psi_4^{(1)} = \frac{2}{\sqrt{6}}\left(\frac{W_x^-}{E_4^{(0)} - E_2^{(0)}}\right)\psi_2^{(0)}$$
$$+ \frac{2}{\sqrt{6}}\left(\frac{W_e\delta^-}{E_4^{(0)} - E_5^{(0)}}\right)\psi_5^{(0)}$$
$$+ \frac{\sqrt{2}}{3}\left(\frac{W_e\delta^+ - W_x^+}{E_4^{(0)} - E_6^{(0)}}\right)\psi_6^{(0)}, \tag{A49}$$

$$\psi_5^{(1)} = \frac{\sqrt{3}}{2}\left(\frac{W_x^-}{E_5^{(0)} - E_3^{(0)}}\right)\psi_3^{(0)}$$
$$+ \frac{2}{\sqrt{6}}\left(\frac{W_e\delta^-}{E_5^{(0)} - E_4^{(0)}}\right)\psi_4^{(0)}$$
$$+ \frac{1}{\sqrt{3}}\left(\frac{W_e\delta^-}{E_5^{(0)} - E_6^{(0)}}\right)\psi_6^{(0)}, \tag{A50}$$

$$\psi_6^{(1)} = \frac{\sqrt{3}}{6} \left(\frac{-W_x^-}{E_6^{(0)} - E_2^{(0)}} \right) \psi_2^{(0)}$$

$$+ \frac{\sqrt{2}}{3} \left(\frac{W_e \delta^+ - W_x^+}{E_6^{(0)} - E_4^{(0)}} \right) \psi_4^{(0)}$$

$$+ \frac{1}{\sqrt{3}} \left(\frac{W_e \delta^-}{E_6^{(0)} - E_5^{(0)}} \right) \psi_5^{(0)}, \qquad (A51)$$

where $\delta^- \equiv [\delta(-1) - \delta(+1)]$ and $W_x^- \equiv (W_{x_2} - W_{x_1})$. One may note that the mixing of the zeroth order eigenvectors by the perturbation depends not only on the mean values of W_{x_1} and W_{x_2} and of $\delta(+1)$ and $\delta(-1)$ but on their differences as well. Hence it might appear that one could determine all of the relevant relaxation rates experimentally by fitting the 2D ELDOR spectrum according to Eq. (A10) while utilizing the perturbed transformation matrix and normal modes described in Eqs. (A39)–(A51). Unfortunately this is not the case in general (e.g., when all of the nonsecular terms are important), because of the invariance of Eq. (A10) to a permutation of indices m and n. In other words the 2D spectrum is symmetric about the diagonal $\omega_1 = \omega_2$ (neglecting off-resonance effects) and there are only three distinct normalized cross-peaks and two distinct normalized autopeaks, in terms of their dependence on the normal modes. Hence a single 2D spectrum is not sufficient to determine the seven relaxation rates W_e, W_n, ω_{HE}, W_{x_1}, W_{x_2}, $\delta(+1)$, and $\delta(-1)$ (nor the six that remain after factoring out W_e). However, all seven relaxation rates can in principle be determined, with the combined analysis of two (or more) 2D ELDOR spectra taken at different mixing times T. This is a result of the fact that the matrix of normalized volumes $\mathbf{Q}(T)$ will be different for the two (or more) spectra, but the transformation matrix of Eq. (A39) will not. Such an analysis would, in general, require the implementation of a nonlinear least-squares algorithm which iterates throughout the parameter space of the seven relaxation rates and satisfies some best fit criterion (usually χ^2) between $\mathbf{Q}(T)$ and the right side of Eq. (A10). This iteration scheme could easily be combined with a matrix diagonalization routine to compute the transformation matrix and the normal modes needed for each state of the fitting. [Alternatively, for isotropic liquids, one could impose the well-known[34] theoretical relations between W_{x_1}, W_{x_2}, $\delta(+1)$, and $\delta(-1)$ in terms of just $J^{DD}(\omega_e)$ and $J^{DG}(\omega_e)$ to reduce the unknown parameters to be fit to just five.]

APPENDIX B: INHOMOGENEOUS BROADENING

A successful double resonance experiment such as 2D ELDOR requires the accurate determination of population differences between spin states. If the longitudinal magnetization is detected by conversion into transverse magnetization, e.g., via a $\pi/2$ microwave pulse, then the population differences are reflected in the amplitudes of the Fourier components of the free induction decay, or alternatively in the areas under the resonance lines. In two dimensional spectroscopy these amplitudes are usually obtained by measurement of volume integrals of autopeaks and cross-peaks. The objective of this appendix is to assess the effect of inhomogeneous broadening in the estimation of peak areas and vol-

ume integrals and hence relaxation rates in the motional narrowing regime by 2D ELDOR and related experiments. Let us assume a signal of the form

$$s(t) = \sum_{j=1}^{3} (O_{1j})^2 \exp(-i\omega_j t) \exp(-t/T_{2j}), \qquad (B1)$$

where the matrix elements $O_{1j} = 1/\sqrt{3}$ are obtained from Eq. (A12). We can incorporate a normalized inhomogeneous weighting function $H(t)$ to reflect the static local fields from unresolved superhyperfine structure in the motional narrowing regime (as well as static distribution of directors in the case of smectogens). We obtain for the observed time domain signal $\hat{s}(t)$ the product of $H(t)$ and $s(t)$

$$\hat{s}(t) = \frac{1}{3} \sum_{j=1}^{3} H(t) \exp(-i\omega_j t) \exp(-t/T_{2j}), \qquad (B2)$$

which upon Fourier transformation with respect to time yields the convolution

$$S(\omega) = \frac{1}{3\pi} \sum_{j=1}^{3} \int_{-\infty}^{\infty} d\omega_\alpha \, h(\omega_\alpha)$$

$$\times \left\{ \frac{T_{2j}^{-1}}{[\omega - (\omega_\alpha + \omega_j)]^2 + T_{2j}^{-2}} \right\}, \qquad (B3)$$

where $h(\omega_\alpha) = \mathscr{F}\{H(t)\}_{\omega_\alpha}$. Integrating the jth hyperfine component of the spectrum with respect to ω gives the expression for the peak area (after some rearrangement)

$$A = \frac{1}{3\pi} \int_{-\infty}^{\infty} d\omega_\alpha \, h(\omega_\alpha)$$

$$\times \int_{-\infty}^{\infty} d\omega \left\{ \frac{T_{2j}^{-1}}{[\omega - (\omega_\alpha + \omega_j)]^2 + T_{2j}^{-2}} \right\},$$

$$= \frac{1}{3} \int_{-\infty}^{\infty} d\omega_\alpha \, h(\omega_\alpha) = \frac{1}{3}, \qquad (B4)$$

which is precisely the result obtained in the absence of inhomogeneous broadening. This result is easily generalized to multiple dimensions. Thus an accurate determination of instantaneous population differences is not influenced by the presence of inhomogeneous broadening in the resonance lines, irrespective of its functional form.

[1] C. F. Polnaszek and J. H. Freed, J. Phys. Chem. **79**, 2283 (1975).
[2] W.-J. Lin and J. H. Freed, J. Phys. Chem. **83**, 379 (1979).
[3] J. H. Freed, J. Chem. Phys. **66**, 4183 (1977).
[4] J. S. Hwang, R. P. Mason, L. P. Hwang, and J. H. Freed, J. Phys. Chem. **79**, 489 (1975).
[5] S. A. Zager and J. H. Freed, Chem. Phys. Lett. **109**, 270 (1984).
[6] J. H. Freed, in *Rotational Dynamics of Small and Macromolecules, Lecture Notes in Physics*, edited by T. Dorfmüller and R. Pecora (Springer, Berlin, 1987), Vol. 293, p. 89.
[7] G. Moro and P. L. Nordio, J. Phys. Chem. **89**, 997 (1985).
[8] P. Pincus, Solid State Commun. **7**, 415 (1969).
[9] P. Ukleja, J. Pirs, and J. W. Doane, Phys. Rev. **14**, 414 (1976).
[10] J. W. Doane, C. E. Tarr, and M. A. Nickerson, Phys. Rev. Lett. **33**, 620 (1974).
[11] C. G. Wade, Annu. Rev. Phys. Chem. **28**, 47 (1977).
[12] T. H. Mugele, V. Graf, W. Wölfel, and F. Noack, Z. Naturforsch. Tei. A **35**, 924 (1980).
[13] R. R. Vold, R.L. Vold, and N. M. Szeverenyi, J. Phys. Chem. **85**, 1934 (1981).

[14]G. Nagele, W. Wölfel, and F. Noack, Isr. J. Chem. **23**, 380 (1983).

[15]L. Plomp, M. Schreurs, and J. Bulthuis, J. Chem. Phys. **88**, 5202 (1988).

[16]F. Noack, M. Notter, and W. Weiss, Liq. Cryst. **3**, 907 (1988).

[17]R. R. Vold and R. L. Vold, J. Chem. Phys. **88**, 4655 (1988).

[18]M. Vilfan, M. Kogoj, and R. Blinc, J. Chem. Phys. **86**, 1055 (1986).

[19]R. Blinc, M. Luzar, M. Vilfan, and M. Burgar, J. Chem. Phys. **63**, 3445 (1975).

[20]R. Blinc, M. Luzar, M. Mali, R. Osredkar, J. Seliger, and M. Vilfan, J. Phys. (Paris) Colloq. **37**, C3-73 (1976).

[21]J. A. Marqusee, M. Warner, and K. A. Dill, J. Chem. Phys. **81**, 6404 (1984).

[22]K. V. S. Rao, J. S. Hwang, and J. H. Freed, Phys. Rev. Lett. **37**, 515 (1976).

[23]A. Nayeem, Ph.D. thesis, Cornell University, 1986; A. Nayeem, S. Rananavare, and J. H. Freed (to be published).

[24]S. B. Rananavare, V. G. K. M. Pisipati, and J. H. Freed, Liq. Cryst. **3**, 957 (1988).

[25]J. H. Freed (to be published).

[26]E. van der Drift, Ph.D. thesis, Delft Technical University, Delft, The Netherlands, 1985.

[27]L. S. Selwyn, R. R. Vold, and R. L. Vold, Mol. Phys. **55**, 287 (1985).

[28]E. Meirovitch, D. Igner, E. Igner, G. Moro, and J. H. Freed, J. Chem. Phys. **77**, 3915 (1982).

[29]J. S. Hwang, K. V. S. Rao, and J. H. Freed, J. Chem. Phys. **80**, 1490 (1976).

[30]R. R. Vold, P. H. Kobrin, and R. L. Vold, J. Chem. Phys. **69**, 3430 (1978); R. Poupko, R. L. Vold, and R. R. Vold, J. Phys. Chem. **84**, 3444 (1980); R. L. Vold and R. R. Vold, Isr. J. Chem. **23**, 315 (1983).

[31]H. C. Jarrell, I. C. P. Smith, P. A. Jovall, H. H. Mantsch, and D. J. Siminovitch, J. Chem. Phys. **88**, 1260 (1988).

[32]J. S. Hyde, J. C. W. Chien, and J. H. Freed, J. Chem. Phys. **48**, 4211 (1968).

[33]C. A. Popp and J. S. Hyde, Proc. Natl. Acad. Sci. **79**, 2559 (1982).

[34]J. H. Freed, in *Multiple Electron Resonance Spectroscopy*, edited by M. Dorio and J. H. Freed (Plenum, New York, 1979), Chap. 3.

[35]E. Meirovitch and J. H. Freed, J. Phys. Chem. **84**, 2459 (1980).

[36]E. van der Drift and J. Smidt, J. Phys. Chem. **88**, 2275 (1984).

[37]R.N. Schwartz, L. L. Jones, and M. K. Bowman, J. Phys. Chem. **83**, 3429 (1979).

[38]A. E. Stillman, L. J. Schwartz, and J. H. Freed, J. Chem. Phys. **73**, 3502 (1980).

[39]L. J. Schwartz, A. E. Stillman, and J. H. Freed, J. Chem. Phys. **77**, 5375 (1982).

[40]J. Gorcester and J. H. Freed, J. Chem. Phys. **85**, 5375 (1986).

[41]J. Gorcester and J. H. Freed, J. Chem. Phys. **88**, 4678 (1988).

[42](a) J. Gorcester and J. H. Freed, J. Magn. Reson. **78**, 292 (1988); (b) The LPSVD results in S2 solvent do indicate *very weak* $\Delta M_l = \pm 2$ peaks, but only at the highest temperatures studied, consistent with a very small Heisenberg exchange at those temperatures.

[43]J. P. Hornak and J. H. Freed, Chem. Phys. Lett. **101**, 115 (1983).

[44]G. Maier and A. Saupe, Mol. Cryst. Liq. Cryst. **1**, 515 (1965).

[45]W. L. McMillan, Phys. Rev. A **4**, 1238 (1971); **6**, 936 (1972).

[46]K. Kobayashi, Mol. Cryst. Liq. Cryst. **13**, 137 (1971).

[47]M. J. Stephen and J. P. Straley, Rev. Mod. Phys. **46**, 617 (1974).

[48]P. J. Wojtowicz, in *Introduction to Liquid Crystals*, edited by E. B. Priestley, P. J. Wojtowicz, and P. Sheng (Plenum, New York, 1975), Chap. 7.

[49]L. P. Hwang and J. H. Freed, J. Chem. Phys. **63**, 118 (1975).

[50]J. H. Freed and G. K. Fraenkel, J. Chem. Phys. **39**, 326 (1963).

[51]S. A. Goldman, G. V. Bruno, C. F. Polnaszek, and J. H. Freed, J. Chem. Phys. **56**, 716 (1972).

[52]P. W. Atkins, in *Electron Spin Relaxation in Liquids*, edited by L. T. Muus and P. W. Atkins (Plenum, New York, 1972).

[53]M. E. Rose, *Elementary Theory of Angular Momentum* (Wiley, New York, 1957).

[54]G. R. Luckhurst and C. Zannoni, Proc. R. Soc. London Ser. A. **353**, 87 (1977).

[55]L. D. Favro, in *Fluctuation Phenomenon in Solids*, edited by R. E. Burgess (Academic, New York, 1965), p. 79.

[56]C. F. Polnaszek, G. V. Bruno, and J. H. Freed, J. Chem. Phys. **58**, 3185 (1973).

[57]G. Moro and P. L. Nordio, Mol. Cryst. Liq. Cryst. **104**, 361 (1984).

[58]R. Schaetzing and J. D. Litster, *Advances in Liquid Crystals* (Clarendon, Oxford, 1979), Vol. 4, p. 147.

[59]G. P. Zientara and J. H. Freed, J. Chem. Phys. **79**, 3077 (1983).

[60]R. Y. Dong, Isr. J. Chem. **23**, 370 (1983), see Ref. 23.

[61]L. Plomp and J. Bulthuis, Liq. Cryst. **3**, 927 (1988).

[62]M. Warner, Mol. Phys. **52**, 677 (1984).

[63]P. G. de Gennes, Solid State Commun. **10**, 573 (1972).

[64]L. Léger and A. Martinet, J. Phys. (Paris) Colloq. **37**, C3-89 (1976).

[65]B. C. Nishida, R. L. Vold, and R. R. Vold, J. Phys. Chem. **90**, 4465 (1986).

[66](a) S. A. Zager and J. H. Freed, J. Chem. Phys. **77**, 3344 (1982); (b) **77**, 3360 (1982).

[67]G. Moro and J. H. Freed, J. Chem. Phys. **74**, 3757 (1981); **75**, 3157 (1981).

[68]L. J. Schwartz, Ph.D. thesis, Cornell University, 1984; L. J. Schwartz and J. H. Freed (to be published).

[69]J. H. Freed, in *Time Domain Electron Spin Resonance*, edited by L. Kevan and R. N. Schwartz (Wiley, New York, 1979).

[70]J. Gorcester, Ph.D. thesis, Cornell University, 1989.

[71]E. Meirovitch and J. H. Freed, J. Phys. Chem. **88**, 4995 (1984).

[72]S. B. Rananavare, V. G. K. M. Pisipati, and J. H. Freed, Chem. Phys. Lett. **140**, 255 (1987).

[73]In our analysis, we have not included any effects from intramolecular motions. In Ref. 4, possible effects of any interconversion between the two twisted boat conformations were considered, since this could modulate the *orientation* of the hyperfine tensor. A twisted boat conformation exists in a single crystal, but no direct evidence has been seen in solution because only one methyl ^{13}C hf coupling constant is observed (Ref. 4). In many careful CW spin–relaxation studies, in particular, those reported in Refs. 4 and 66(b), where different solvents were studied as a function of temperature and pressure, no spin–relaxation could be detected which could be attributed to any residual contributions from intramolecular processes, since such a process would obey very different dependences on viscosity, temperature, and pressure than exhibited for the overall molecular reorientation.

[74]C. F. Polnaszek, Ph.D. thesis, Cornell University, 1976.

[75]See Ref. 3, Table I; these results are for isotropic Brownian diffusion.

[76]P. de Gennes, *The Physics of Liquid Crystals* (Oxford, Oxford, 1974).

[77]G. J. Krüger, Phys. Rep. **82**, 230 (1982).

[78]J. P. Hornak, J. K. Moscicki, D. J. Schneider, and J. H. Freed, J. Chem. Phys. **84**, 3387 (1986).

[79]N. Boden, L. D. Clark, R. J. Bushby, J. W. Emsley, G. R. Luckhurst, and C. P. Straley, Mol. Phys. **42**, 565 (1981).

[80]C. J. R. Counsell, J. W. Emsley, G. R. Luckhurst, and H. S. Sachdev, Mol. Phys. **63**, 33 (1988).

[81]J. H. Freed, J. Phys. Chem. **71**, 38 (1967).

[82]Thus, the effect of quadrupole relaxation would be to contribute directly to the intensity of both the $\Delta M_L = \pm 1$ and $\Delta M_L = \pm 2$ cross peaks.

[83]E. Merzbacher, *Quantum Mechanics*, 2nd ed. (Wiley, New York, 1970).

[84]Strictly speaking, one must also correct the observed FID for the limited bandwidth of the resonator as referred to in Sec. II D of Ref. 41. However, the method given above for determining $V_i r_2$ automatically includes this correction.